HHS Public Access

Author manuscript

Cell. Author manuscript; available in PMC 2024 July 28.

Published in final edited form as:

Cell. 2024 July 25; 187(15): 4061–4077.e17. doi:10.1016/j.cell.2024.05.034.

NLRC5 senses NAD+ depletion to form a PANoptosome driving PANoptosis and inflammation

Balamurugan Sundaram[1,#], **Nagakannan Pandian**[1,#], **Hee Jin Kim**[1], **Hadia M. Abdelaal**[1], **Raghvendra Mall**[1,2], **Omkar Indari**[1], **Roman Sarkar**[1], **Rebecca E. Tweedell**[1], **Emily Q. Alonzo**[3], **Jonathon Klein**[4], **Shondra M. Pruett-Miller**[4], **Peter Vogel**[5], **Thirumala-Devi Kanneganti**[1,*]

[1]Department of Immunology, St. Jude Children's Research Hospital, Memphis, TN, 38105, USA

[2]Current affiliation: Biotechnology Research Center, Technology Innovation Institute, Abu Dhabi, P.O. Box 9639, United Arab Emirates

[3]Department of Research and Development, Cell Signaling Technology, Danvers, MA, 01915, USA

[4]Center for Advanced Genome Engineering, St. Jude Children's Research Hospital, Memphis, Tennessee, 38105, USA

[5]Animal Resources Center and the Veterinary Pathology Core, St. Jude Children's Research Hospital, Memphis, TN, 38105, USA

SUMMARY

NLRs are a large, highly conserved family of cytosolic pattern recognition receptors that are central to health and disease and serve as key therapeutic targets. NLRC5 is an enigmatic NLR, with mutations associated with inflammatory and infectious diseases, but little is known about its function as an innate immune sensor and cell death regulator. Therefore, we screened for NLRC5's role in response to infections, PAMPs, DAMPs, and cytokines. We identified that NLRC5 drives the innate immune cell death pathway, PANoptosis, in response to specific ligands, including PAMP/DAMP (heme) and DAMP/cytokine combinations. NLRC5 interacted

[*]Lead contact: Thirumala-Devi Kanneganti, Department of Immunology, St. Jude Children's Research Hospital, MS #351, 262 Danny Thomas Place, Memphis, TN 38105-3678, Fax: (901) 595-5766, Thirumala-Devi.Kanneganti@StJude.org.

[#]These authors contributed equally to this work.

AUTHOR CONTRIBUTIONS

B.S., N.P., and T.-D.K. conceptualized the study; B.S. and N.P. designed the methodology; B.S., N.P., O.I., and R.S. performed the experiments; B.S. and N.P. performed in vitro and in vivo data analysis; R.M. conducted the gene expression and publicly available dataset analysis; H.M.A. performed the confocal microscopy; H.J.K. performed the immunoprecipitation analyses; R.E.T. performed data analysis and interpretation; E.Q.A. performed the NLRC5 antibody generation and validation; J.K. and S.M.P.-M. created the new *Nlrc5* knockout mouse; P.V. performed additional in vivo analyses; B.S. wrote the manuscript with input from all authors. T.-D.K. acquired the funding and provided overall supervision.

DECLARATION OF INTERESTS

St. Jude Children's Research hospital filed a provisional patent application on methods for modulating NLRP12 and NLRC5 described in this study, listing B.S. and T.-D.K. as inventors (serial no. 63/501,430). The PCT application was published with the World Intellectual Property Organization (WO 2024/097571 A1).

with NLRP12 and PANoptosome components to form a cell death complex, suggesting an NLR network, like those in plants, forms with NLRC5 and NLRP12. TLR signaling and NAD^+ levels regulated NLRC5 expression and ROS production to control cell death. NLRC5-deficient mice were protected in hemolytic and inflammatory models, suggesting that NLRC5 could be a potential therapeutic target.

GRAPHICAL ABSTRACT

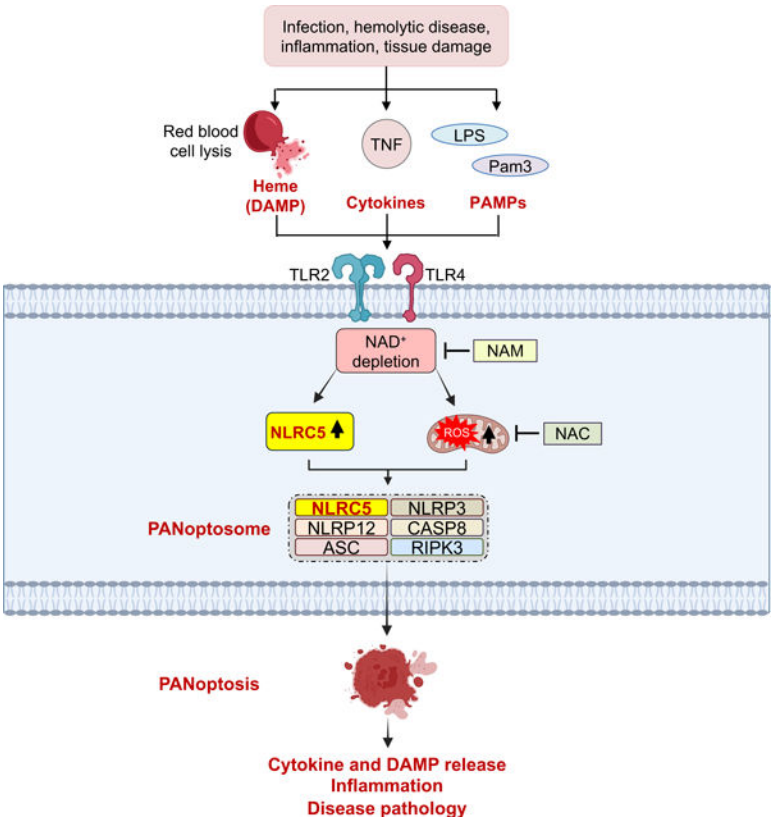

Keywords

NLRC5; NLRP12; heme; hemolysis; colitis; hemophagocytic lymphohistiocytosis; PAMP; DAMP; Pam3CSK4; LPS; poly(I:C); TNF; phenylhydrazine; DSS; creatinine; nicotinamide adenine dinucleotide; ROS; inflammasome; NLRP3; inflammatory cell death; pyroptosis; apoptosis; necroptosis; PANoptosis; PANoptosome; gasdermin E; gasdermin D; caspase; caspase-1; caspase-8; caspase-3; caspase-7; ASC; RIPK3; MLKL; TLRs; TLR2; TLR4; inflammation

INTRODUCTION

Innate immunity is the critical first line of defense against infection and sterile insults. The innate immune system relies on pattern recognition receptors (PRRs) to sense various pathogen-associated and damage-associated molecular patterns (PAMPs and DAMPs) and induce inflammatory signaling pathways[1]. While PRRs are central to host defense,

polymorphisms in these sensors can lead to severe autoinflammatory diseases and other disease susceptibilities. One such family of cytosolic PRRs is the NLRs, which are highly evolutionarily conserved and have been found to be critical for inflammatory signaling[1–3]. Given the growing understanding of the impact of NLRs in health and disease, they are often considered as therapeutic targets. However, the function of many NLRs in innate immunity, including their activating triggers, downstream pathways, and roles in inducing cell death and inflammation, remain unknown.

NLRC5 is one of the most enigmatic NLRs, and it is highly expressed in hematopoietic cells[4]. NLRC5 is also known as MHC class I transactivator (CITA) and is best characterized as a molecule that translocates between the nucleus and cytoplasm to regulate transcription of MHC class I genes[4,5]. Decreased expression of *NLRC5* is linked to impaired $CD8^+$ T-cell activation and poor patient prognosis in different cancer types[6], and polymorphisms in NLRC5 can affect susceptibility to chronic periodontitis and pulmonary aspergillosis[7,8], highlighting its key connections to disease. In addition to regulating the expression of MHC class I genes, NLRC5 is associated with NLRP3 inflammasome activation in response to bacterial infection, PAMPs, and DAMPs[9]. Furthermore, NLRC5 negatively regulates NF-kB and type I IFN signaling in response to vesicular stomatitis virus (VSV) infection[10]. However, despite over 20 years of research, beyond its role in regulating MHC-I expression and limited signaling pathways, little is known about NLRC5's functions in inflammation and cell death regulation. Given the associations between polymorphisms in *NLRC5* and susceptibility to infectious and inflammatory diseases[7,8], as well as cancers[6], understanding NLRC5 is essential for developing potential therapeutic interventions.

In this study, we investigated the critical functions of NLRC5 in innate immunity by performing an unbiased screen of its role in cell death in response to infections, PAMPs, DAMPs, cytokines, and physiologically relevant combinations thereof. We identified that NLRC5 drives inflammatory cell death in response to specific ligands, including PAMP/DAMP (heme) and DAMP/cytokine combinations. TLR signaling and nicotinamide adenine dinucleotide (NAD^+) levels drove the NLRC5 expression and ROS production necessary for cell death. Furthermore, NLRC5 associated with NLRP12 and cell death molecules to form an NLRC5-PANoptosome complex that triggered this inflammatory cell death. These connections between NLRs suggests that the NLR network concept previously identified in plants[11] may be evolutionarily conserved and occur with NLRC5 and NLRP12. Moreover, *Nlrc5*$^{-/-}$ mice were protected from inflammation, tissue damage, and lethality in a sterile hemolytic disease model, as well as colitis and hemophagocytic lymphohistiocytosis (HLH) models. Altogether, we identified NLRC5 as a critical NLR sensor that responds to PAMP/DAMP (heme) and DAMP/cytokine combinations to drive innate immune cell death, PANoptosis, and contribute to inflammatory disease pathology, implicating NLRC5 and the molecules involved in this pathway as potential targets to alleviate inflammation and disease severity.

RESULTS

NLRC5 is required for lytic cell death

NLRC5 remains a highly enigmatic innate immune molecule, and the specific triggers that activate NLRC5 and its roles in driving inflammatory cell death are unknown. Therefore, we performed an unbiased screen of WT and *Nlrc5*$^{-/-}$ bone marrow-derived macrophages (BMDMs) for cell death in response to a variety of infections, PAMPs, DAMPs, and cytokines. We found no significant difference in cell death between WT and *Nlrc5*$^{-/-}$ BMDMs in response to infections with influenza A virus (IAV), *Salmonella enterica* serovar Typhimurium, or *Escherichia coli* (Figures S1A–S1F). Furthermore, we tested canonical inflammasome triggers and found no significant reduction in cell death in *Nlrc5*$^{-/-}$ BMDMs compared with WT BMDMs in response to poly(dA:dT) transfection or LPS transfection (Figures S1G–S1J) or in response to LPS plus ATP (Figures S2A and S2B). In addition to these canonical triggers, a recent study identified a new inflammatory cell death trigger, PAMP plus heme combinations[12]. Heme is a crucial DAMP which can be released upon hemolysis in various inflammatory and hemolytic diseases, and excess circulating heme can cause severe inflammation and organ damage[13–15]. We found that cell death was significantly decreased in *Nlrc5*$^{-/-}$ BMDMs in response to heme plus LPS (Figures 1A and 1B), heme plus R848 (Figures 1C and 1D), and heme plus Pam3 treatment (Figures S2C and S2D), indicating that NLRC5 is required to induce heme plus PAMP-mediated inflammatory cell death. Previous studies have reported that cell death can also be driven in response to heme plus TNF[12,16,17]. We found that *Nlrc5*$^{-/-}$ BMDMs underwent significantly reduced cell death in response to heme plus TNF compared with WT BMDMs (Figures 1E and 1F).

We next determined whether the NLRC5-mediated cell death we observed in murine macrophages in response to heme plus PAMP stimulation also occurred in human cells. Heme plus LPS stimulation induced cell death in human monocyte-derived macrophages treated with non-targeting siRNA, while there was a significant decrease in cell death in macrophages treated with *NLRC5*-targeting siRNA (Figures S2E–S2G). Moreover, we also observed increased expression of NLRC5 in non-targeting siRNA-treated human macrophages in response to heme plus LPS (Figure S2G). These data suggest that NLRC5 is critical for inflammatory cell death in human macrophages in response to heme plus PAMP triggers.

Beyond heme combinations and inflammasome triggers, other PAMP plus PAMP combinations have also been shown to induce inflammatory cell death[12]. We therefore assessed whether NLRC5 was required for cell death in response to PAMP plus PAMP combinations. However, *Nlrc5*$^{-/-}$ BMDMs were not protected against inflammatory cell death in response to R848 plus poly(I:C) treatment (Figures S2H and S2I). Overall, these results suggest that NLRC5 is required for inflammatory cell death in response to specific PAMP plus DAMP and DAMP plus cytokine combinations.

To further confirm the importance of NLRC5 in inflammatory cell death, we used siRNA to silence *Nlrc5* in WT BMDMs. Consistent with our observations in *Nlrc5*$^{-/-}$ BMDMs, we found that treatment with *Nlrc5* siRNA significantly reduced cell death compared to

non-targeting siRNA treatment in WT BMDMs in response to heme plus PAMPs (Figures 1G–1I). To provide an additional line of genetic evidence, we generated a new *Nlrc5* knockout (KO) mouse using CRISPR-Cas9 technology, referred to here as *Nlrc5*-KO^{line2} (Figures S3A–S3C). Using littermate controls from the newly generated *Nlrc5*-KO^{line2} line, we observed significantly decreased cell death in *Nlrc5*-KO^{line2} BMDMs compared to littermate *Nlrc5*$^{+/+}$ BMDMs in response to heme plus Pam3 (Figures 1J and 1K). Together, these data suggest that NLRC5 acts as a critical NLR sensor to induce inflammatory cell death in response to specific ligands.

NLRC5 drives innate immune cell death, PANoptosis, in response to its specific ligands

Innate immune activation in response to heme plus PAMP combinations induces PANoptosis, a unique lytic, innate immune, inflammatory cell death pathway initiated by innate immune sensors and driven by caspases and RIPKs through PANoptosome complexes[12]. We therefore assessed the effect of NLRC5 on activation of PANoptosis molecules. While activation of caspase-1 was comparable between WT and *Nlrc5*$^{-/-}$ BMDMs (Figure 2A), caspase-1 activation in response to heme plus PAMP treatment was previously shown to be driven by NLRP12 and NLRP3[12]. To confirm whether this was the case in *Nlrc5*$^{-/-}$ BMDMs, we used the NLRP3 inhibitor, MCC950[18]. The activation of caspase-1 was similarly decreased in MCC950-treated WT and *Nlrc5*$^{-/-}$ BMDMs (Figure S4A), indicating that the activation of caspase-1 was dependent on NLRP3, but not NLRC5, in response to heme plus Pam3. However, MCC950 treatment did not have any significant effect on cell death in WT and *Nlrc5*$^{-/-}$ BMDMs following treatment with heme plus PAMPs (Figures S4B and S4C), suggesting that while NLRP3 was required for caspase-1 activation, NLRP3 did not have an effect on the cell death.

In contrast to caspase-1, we found that the cleavage of gasdermin D (GSDMD) (especially the P20 form) and the activation of GSDME, caspases-8, −3, and −7, and MLKL were reduced in *Nlrc5*$^{-/-}$ BMDMs compared with WT BMDMs following treatment with heme plus Pam3 (Figures 2A–2C), suggesting that NLRC5 regulated the activation of PANoptosis molecules to drive inflammatory cell death. Moreover, MCC950 treatment did not reduce the cleavage of GSDMD to its P20 form or the activation of GSDME in WT and *Nlrc5*$^{-/-}$ BMDMs following heme plus PAMPs stimulation (Figures S4A); this is consistent with the known role of caspase-3, rather than NLRP3-mediated caspase-1, in cleaving GSDMD to its P20 form and inactivating GSDMD[19].

Previous work has shown that NLRP12 is an innate immune sensor that drives heme plus PAMP-mediated inflammatory cell death[12]. To determine the relationship between NLRC5 and NLRP12 in regulating this cell death, we generated *Nlrc5*$^{-/-}$*Nlrp12*$^{-/-}$ double knockout (DKO) mice. *Nlrp12*$^{-/-}$ and *Nlrc5*$^{-/-}$*Nlrp12*$^{-/-}$ BMDMs were similarly protected from cell death (Figures 2D and 2E). We also observed slightly more cell death in *Nlrc5*$^{-/-}$ BMDMs compared with *Nlrp12*$^{-/-}$ or *Nlrc5*$^{-/-}$ *Nlrp12*$^{-/-}$ BMDMs (Figures 2D and 2E). Together, these results suggest that NLRC5 could be in the same pathway or in the same complex together with NLRP12 to drive heme plus PAMP-mediated inflammatory cell death.

To further understand the molecular relationship between NLRC5 and NLRP12 in regulating inflammatory cell death, we investigated how the loss of both NLRC5 and NLRP12 (*Nlrc5*$^{-/-}$ *Nlrp12*$^{-/-}$) molecularly impacted cell death. Consistent with our earlier observation (Figure 2A), activation of caspase-1 was comparable between WT and *Nlrc5*$^{-/-}$ BMDMs in response to heme plus Pam3 (Figure 2F); however, caspase-1 activation was decreased in *Nlrp12*$^{-/-}$ and *Nlrc5*$^{-/-}$ *Nlrp12*$^{-/-}$ BMDMs (Figure 2F). Similarly, there was comparable release of IL-1β between WT and *Nlrc5*$^{-/-}$ BMDMs, but a trend toward reduction in IL-1β release in *Nlrp12*$^{-/-}$*Nlrc5*$^{-/-}$ BMDMs compared with WT BMDMs at 36 h post-treatment and a significant reduction at 42 h post-treatment (Figure 2G). Combined with our previous observations using MCC950, these results suggest that caspase-1 activation is driven by NLRP12 (Figure 2F) and NLRP3 (Figure S4A) in response to heme plus Pam3 stimulation. Furthermore, we observed similar decreases in the cleavage of GSDMD (P20 form) and activation of GSDME, caspases-8, −3, and −7, and MLKL in *Nlrc5*$^{-/-}$, *Nlrp12*$^{-/-}$, and *Nlrc5*$^{-/-}$*Nlrp12*$^{-/-}$ BMDMs compared with WT BMDMs (Figure 2F). Together, these results show that both NLRC5 and NLRP12 regulated the activation of inflammatory cell death, whereas NLRP12 and NLRP3 regulated the activation of caspase-1. These results suggest that NLRC5 could interact with NLRP3 and NLRP12 to drive PANoptosis in response to its specific ligands.

NLRC5 interacts with NLRP12 and cell death molecules to drive PANoptosis

Since we observed a decrease in the activation of cell death molecules and a reduction in the frequency of inflammatory cell death in the absence of NLRC5 (Figures 1, 2A–2C, and 2F), we next examined whether NLRC5 impacted the formation of the PANoptosome in response to heme plus PAMPs. We observed increased expression of NLRC5 by immunofluorescence (Figure 3A) and immunoblotting (Figure 3B) in response to heme plus Pam3. We also observed co-localization of the key PANoptosome molecules ASC, caspase-8, and RIPK3 together with NLRC5 in WT BMDMs following treatment with heme plus Pam3 (Figures 3C and 3D), suggesting that NLRC5 is required to form the PANoptosome complex. Previous work has shown that NLRP12 interacts with ASC, caspase-8, and RIPK3 to drive PANoptosis in response to heme plus PAMPs[12]. To determine the role of NLRC5 in this complex, we performed endogenous immunoprecipitation in WT, *Nlrp12*$^{-/-}$, *Pycard*$^{-/-}$, and *Nlrc5*$^{-/-}$ BMDMs following heme plus Pam3 treatment. We observed the formation of a multiprotein complex containing NLRC5, ASC, RIPK3, caspase-8, and NLRP3 in WT BMDMs, and the formation of this complex was abolished in the absence of NLRP12, ASC, or NLRC5 (Figure 3E). These results suggest that NLRC5, as well as NLRP12 and ASC, are integral components of the PANoptosome complex to drive PANoptosis in response to heme plus PAMP stimulation. In an overexpression system, we also pulled down a multiprotein complex containing NLRP12, ASC, NLRC5, caspase-8, RIPK3, and NLRP3, though NLRP3 was not required for the complex formation (Figure S5A). Together, these results suggest that NLRC5 forms a PANoptosome complex with NLRP12 that drives heme plus PAMP-mediated inflammatory cell death.

Membrane bound TLR- and NAD$^+$-mediated regulation of NLRC5 expression and ROS production modulate PANoptosis

Given the critical role we observed for NLRC5 in driving inflammatory cell death (Figures 1, 2A–2C, and 2F) and its upregulated expression following heme plus PAMPs stimulation (Figures 3A and 3B), we next examined the expression of NLRC5 in hemolytic diseases such as malaria or sickle cell disease (SCD). Using publicly available datasets[20–23], we observed that the expression of *NLRC5* was significantly upregulated in whole blood (WB) and CD71$^+$ cells from patients with malaria and in SCD monocytes compared to healthy donors (Figure S5B), suggesting that hemolysis and circulating free heme are associated with increased expression of NLRC5. Moreover, NLRC5 protein expression was increased in response to heme or Pam3 alone (Figure S5C), suggesting that both heme and Pam3 signaling can induce NLRC5 expression. Taken together, these results indicate that the expression of NLRC5 is increased by heme plus PAMP treatment, and this increase is associated with hemolytic disease.

Next, we sought to determine the upstream signaling pathways responsible for increasing NLRC5 expression and driving cell death in response to heme plus PAMPs. TLR signaling is a common upstream mechanism that controls the expression of innate immune molecules to drive cell death. Heme is known to activate TLR4 signaling[24], and TLR2 has been previously shown to be activated in response to Pam3[25,26]. We found that heme treatment did not induce NLRC5 expression in *Tlr4*$^{-/-}$ and *Tlr2*$^{-/-}$/*4*$^{-/-}$ BMDMs (Figure S5D), while Pam3 treatment did not induce NLRC5 expression in *Tlr2*$^{-/-}$ and *Tlr2*$^{-/-}$/*4*$^{-/-}$ BMDMs (Figure S5E), indicating that, depending on the stimulus, either TLR2 or TLR4 signaling is required for NLRC5 expression. Moreover, this suggests that NLRC5 expression alone is not sufficient to induce cell death, as heme alone and Pam3 alone do not induce cell death[12]. In response to the combined treatment with heme plus Pam3, the expression of NLRC5 was partially decreased in *Tlr2*$^{-/-}$ or *Tlr4*$^{-/-}$ BMDMs, whereas the expression was almost completely abolished in *Tlr2*$^{-/-}$/*4*$^{-/-}$ BMDMs when compared with WT BMDMs (Figure 4A). Moreover, consistent with previous observations[12], the incidence of cell death was significantly decreased in *Tlr2*$^{-/-}$, *Tlr4*$^{-/-}$, and *Tlr2*$^{-/-}$/*4*$^{-/-}$ BMDMs when compared with WT BMDMs in response to heme plus Pam3 (Figure 4B).

Based on this observation that NLRC5 expression was necessary, but not sufficient, to drive cell death, we sought to identify other regulatory processes. Previously, it was shown that TLR-dependent ROS production is also critical for inducing inflammatory cell death in response to heme plus PAMPs[12]. Indeed, treatment with the ROS scavenger N-acetyl cysteine (NAC) significantly reduced cell death in WT BMDMs in response to heme plus Pam3 treatment (Figures S5F and S5G). Moreover, the low level of residual cell death that occurred in *Nlrc5*$^{-/-}$ BMDMs could be further inhibited by treatment with NAC (Figures S5F and S5G), indicating that ROS produced in *Nlrc5*$^{-/-}$ BMDMs can still drive cell death. Additionally, we did not observe any difference in NLRC5 expression in the presence or absence of NAC in response to heme plus PAMPs (Figures S5H), suggesting that NLRC5 expression is independent of ROS production. Together, these data suggest that heme plus PAMP stimulation activates TLR2/4 intracellular signaling pathways that lead to ROS

generation and the upregulation of NLRC5 expression, which are both required for the cell death.

Next, we investigated the mechanisms driving ROS generation and NLRC5 expression in response to heme plus PAMPs. It is known that increased mitochondrial ROS production is proportional to increased mitochondrial respiration[27]. During cellular respiration, NAD^+ (nicotinamide adenine dinucleotide) is a key electron carrier used to temporarily store energy. Mitochondrial NAD^+ levels determine cell viability[28], and depletion of NAD^+ can induce cell death[29–31]. Furthermore, multiple TLR-binding PAMPs are associated with increased expression of NAD^+- consuming enzymes and increased NADase activity, leading to decreased NAD^+ levels in BMDMs[32]. Moreover, in response to LPS, ROS production and NAD^+ depletion have been linked[33], and plant NLR Toll/interleukin-1 receptor (TIR) domains can degrade NAD^+ and induce cell death[34,35]. We therefore hypothesized that stimulation with heme plus PAMPs may trigger NAD^+ depletion, mitochondrial damage, and ROS production to induce NLRC5-mediated inflammatory cell death. To test this hypothesis, we supplemented BMDMs with nicotinamide (NAM), which can be converted into NAD^+ through a salvage pathway[36] and decrease mitochondrial oxidative stress and ROS production in primary human fibroblasts[37,38]. NAM treatment significantly protected BMDMs from cell death in response to heme plus Pam3 (Figures 4C and 4D). Moreover, we also observed decreased activation of many PANoptosis molecules upon treatment with NAM in response to heme plus Pam3, with the exception of caspase-1 (Figure 4E). This is similar to our observations in *Nlrc5*$^{-/-}$ BMDMs (Figures 2A and 2F).

Next, we assessed the effect of NAM on NLRC5 expression. In the presence of NAM, we observed that NLRC5 expression was not upregulated in response to heme, and it was delayed in response to Pam3 and heme plus Pam3 treatments (Figures 4F–4H). Together, these data suggest that NAD^+ levels are key in regulating the expression of NLRC5 and the subsequent cell death.

To connect our observations that NAD^+ levels and ROS production were both involved in heme plus PAMP-mediated inflammatory cell death, we next assessed whether treatment with NAM would impact ROS production. We observed that ROS production was comparable between WT and *Nlrc5*$^{-/-}$ BMDMs in response to heme plus Pam3 stimulation (Figures 4I), suggesting that NLRC5 is not required for ROS production. Additionally, treatment with NAC or NAM significantly reduced ROS production in both WT and *Nlrc5*$^{-/-}$ BMDMs in response to heme plus Pam3 (Figure 4I), suggesting that NAD^+ levels may regulate ROS production as well as NLRC5 expression. Furthermore, treatment with NAC (Figures S5F and S5G) or NAM (Figures 4C and 4D) significantly reduced cell death in WT BMDMs in response to heme plus Pam3, with NAM providing nearly complete protection, while some residual cell death still occurred during NAC treatment. This is likely due to the fact that NAC only regulated ROS production, while NAM regulated NLRC5 expression along with ROS production. Taken together, these data indicate that membrane-bound TLRs and NAD^+ signaling trigger increased expression of NLRC5 and increased cellular ROS generation to induce PANoptosis in response to heme plus Pam3.

NLRC5 triggers acute kidney injury in hemolytic disease

To determine whether NLRC5 mediated disease pathogenesis, we used a previously established model of hemolytic disease[12], in which mice are treated with phenylhydrazine (PHZ), a known inducer of hemolysis[39], along with a sub-lethal LPS dose. *Nlrc5*$^{-/-}$ mice were significantly protected from lethality compared with WT mice following PHZ plus LPS treatment (Figure 5A). However, blood urea nitrogen (BUN) levels were similarly increased in both groups (Figure S6A). Moreover, there were no significant differences observed in serum iron levels and total red blood cell (RBC) count between WT and *Nlrc5*$^{-/-}$ mice in response to PHZ plus LPS (Figures S6B and S6C), suggesting that similar levels of hemolysis were occurring in both groups. Furthermore, we also observed comparable levels of liver damage markers such as serum alanine transaminase (ALT) and serum aspartate aminotransferase (AST) (Figures S6D and S6E) between WT and *Nlrc5*$^{-/-}$ mice in response to PHZ plus LPS. Earlier studies have reported that NLRC5 is involved in driving inflammation and kidney damage in response to ischemia/reperfusion and diabetes models[40,41]; therefore, we focused our subsequent analyses on kidney tissue in the PHZ plus LPS hemolytic disease model. Hematoxylin and eosin (H&E) staining in kidney tissues showed increased tissue damage in WT mice compared with *Nlrc5*$^{-/-}$ mice in response to PHZ plus LPS (Figures 5B and S6F). Consistent with the differences in kidney tissue damage observed by H&E staining, there was also a significant reduction in the levels of the kidney damage marker creatinine in *Nlrc5*$^{-/-}$ mice (Figure 5C). The expression of NLRC5 was also significantly increased in WT kidney tissues after PHZ plus LPS treatment when compared to the control PBS-treated group (Figures 5D and 5E). Lipocalin 2 (LCN2; or neutrophil gelatinase-associated lipocalin (NGAL)) is another kidney damage marker that is increased in kidney diseases[42,43]; we observed increased staining of LCN2 in WT kidney tissues following PHZ plus LPS treatment when compared to the control PBS-treated group (Figures 5F and S6G). Furthermore, there was a significant decrease in the expression of LCN2 in *Nlrc5*$^{-/-}$ kidney tissues compared with those from WT mice (Figures 5F–5H and S6G). Consistently, we also observed decreased activation of caspase-3 and caspase-7 in *Nlrc5*$^{-/-}$ kidney tissues compared with WT kidney tissues in response to PHZ plus LPS (Figures 5G and 5I), suggesting that NLRC5-mediated cell death is playing a critical role in driving inflammation and tissue damage in response to PHZ plus LPS.

Beyond the role we identified for NLRC5 in regulating inflammatory cell death, NLRC5's regulation of MHC class I expression is also known to be critical for CD8^{+} T cell-mediated killing of various cell types, including lymphocytes and cancer cells[6,44]. Therefore, we assessed whether NLRC5-mediated regulation of MHC class I expression and CD8^{+} T cell-mediated cytotoxicity played a role in vivo. We measured comparable numbers of CD8^{+} T cells in WT and *Nlrc5*$^{-/-}$ kidney tissue (Figure S6H). Moreover, we also measured a significant decrease in the number of CD8^{+} T cells in WT and *Nlrc5*$^{-/-}$ PHZ plus LPS-treated mice when compared to WT PBS-treated mice (Figure S6H), suggesting that there may be a limited contribution from CD8^{+} T cells in driving tissue damage or inflammation in the PHZ plus LPS model of hemolytic disease.

Taken together, these results suggest that NLRC5-mediated cell death and inflammation plays a key role in driving acute kidney damage and pathology that contribute to lethality in a hemolytic disease model.

NLRC5 induces inflammation and lethality in colitis and hemophagocytic lymphohistiocytosis models

To determine whether NLRC5 was also involved in pathogenesis during other diseases associated with inflammation, we assessed its role in an acute dextran sodium sulfate (DSS)-induced colitis model[45–47] and an hemophagocytic lymphohistiocytosis (HLH) model. In the colitis model, we measured significantly decreased RBC and hemoglobin (Hb) levels in both WT and *Nlrc5*$^{-/-}$ mice treated with DSS when compared with the WT PBS-treated group (Figures S6I and S6J), suggesting that similar levels of hemolysis occur in both WT and *Nlrc5*$^{-/-}$ mice in response to DSS treatment. We observed that WT mice lost significantly more weight and were more susceptible to DSS-induced lethality when compared with *Nlrc5*$^{-/-}$ mice (Figures 6A and 6B). While we did not observe significant changes in the colon length between WT and *Nlrc5*$^{-/-}$ mice (Figures 6C and 6D), we did observe significantly decreased ulceration and extent of inflammation in *Nlrc5*$^{-/-}$ colon tissues compared with those from WT mice (Figures 6E–6J). Ulceration can be a downstream effect of cell death and cellular membrane damage[48], suggesting that NLRC5-mediated cell death has a role in the inflammation and pathology in acute colitis. Moreover, we also observed increased expression of NLRC5 in response to DSS treatment (Figures 6K and 6L), suggesting further links between NLRC5 and the disease phenotype. Overall, these results suggest that NLRC5 is involved in driving inflammation and tissue damage in acute colitis.

To further expand our understanding of the role of NLRC5 across the disease spectrum, we also assessed its effects in a murine model of HLH, an inflammatory disease that can be induced by treatment with poly(I:C) plus LPS[49 50]. Consistent with our observations in the PHZ plus LPS and colitis models, we observed that NLRC5-deficient mice were significantly protected from lethality in response to poly(I:C) plus LPS injection (Figure S6K), suggesting that NLRC5 plays a critical role in driving pathophysiology in HLH. Collectively, our in vivo results indicate that NLRC5 is involved in driving inflammation and tissue damage in hemolytic, colitis, and HLH disease models.

DISCUSSION

The NLRs are a large, highly evolutionarily conserved family of cytosolic innate immune sensors with diverse functions in health and disease[1–3]. Molecules in this family share a nucleotide-binding domain (NBD) and a leucine-rich repeat (LRR) domain, and different members of the family can carry other accessory domains[51,52]. These proteins can be functionally classified as NLRs that regulate, such as those controlling inflammatory signaling through positive or negative regulation of NF-kB and MAPK pathways or controlling transcription; NLRs that form inflammasomes to induce IL-1β and IL-18 maturation; and NLRs that form larger multiprotein cell death complexes, PANoptosomes[1,12,51–53]. Many of the NLR functions are dictated by the protein

domains present, as these drive specific protein-protein interactions[52]. For instance, the inflammasome-forming NLRs contain pyrin domains or caspase activation and recruitment domains (CARDs) to interact with the adaptor ASC and promote complex formation[54]. However, despite 20 years of research on the NLR proteins, some still have domains with unknown functions. One such NLR is NLRC5, which contains a CARD-like domain, but the functions of this remain uncertain. While NLRC5 is known to regulate the transcription of MHC class I genes[4,5], conflicting roles in the regulation of inflammatory pathways have been observed[9,10,55,56], and its broader functions in inflammasome activation and cell death have remained unclear.

In the context of disease, enhanced immune activation can lead to severe inflammation, tissue damage, and pathology. Identification of the innate immune sensors and regulators that trigger this inflammation is critical to provide new drug targets to alleviate severe inflammation and tissue damage and improve patient outcomes. In the current study, we screened multiple infections, PAMPs, DAMPs, and cytokines to identify NLRC5 as a critical NLR sensor that drives PANoptosis and tissue damage in inflammatory diseases. In the absence of NLRC5, inflammation and disease severity were reduced in hemolytic and colitis disease models, and lethality was reduced in an HLH model of inflammation. Previous reports have suggested intricate connections between hemolysis, the release of PAMPs and DAMPs, and inflammation across the disease spectrum. In hemolytic diseases, this is well known, as multiple studies have observed increased inflammation and tissue damage in this context[57]. However, the connections between hemolysis, PAMP/DAMP release, and inflammation are increasingly apparent in inflammatory and infectious diseases as well[58–62]. Our results suggest that NLRC5 may be responsible for driving this pathology. Furthermore, mutations in NLRC5 are associated with chronic periodontitis and pulmonary aspergillosis[7,8], two conditions associated with hemolysis and the synergistic presence of PAMPs and DAMPs[63,64], further suggesting that NLRC5 may play a role in driving severe inflammation, tissue damage, and pathogenesis in disease.

Our study also suggests that NLRC5 interacts with NLRP12, NLRP3, and other cell death molecules to form the NLRC5-PANoptosome complex that triggers inflammatory cell death. In plants, NLR networks have been extensively described in host defense and the activation of hypersensitive response (HR)-mediated cell death[65–69]. While some NLRs can function as direct sensors and activators of downstream immune signaling, many others have evolved more specialized, divided functions that rely on a network of separate sensor NLRs and helper NLRs that drive the signaling and cell death[11,70]. This allows functional redundancy among helper NLRs. Parallels to these plant NLR networks are also emerging in mammals, with the NAIP-NLRC4 network being the most classical example. In this system, NAIPs act as the sensor NLRs, and NLRC4 acts as the helper NLR to drive cell death [71–75]. Our findings suggest that NLRC5, NLRP12, and NLRP3 are involved in another NLR network.

The existence of an NLR network containing NLRC5, NLRP12, and NLRP3, with functional redundancies between them, may have distinct implications across different cell types. For instance, *Nlrp12*$^{-/-}$ mice have more severe colitis in response to DSS treatment[76,77], while our study shows that *Nlrc5*$^{-/-}$ mice have less inflammation and pathology in this model, despite the observation that NLRC5 and NLRP12 interacted to

form a cell death complex in BMDMs. This could be due to differences in expression patterns and the multifaceted roles of NLRP12 across different cell types. While our findings show NLRP12 was a key component of the NLRC5-PANoptosome in macrophages, NLRP12 also has critical roles in maintaining intestinal homeostasis and regulating the gut microbiome to limit inflammation[76–79]. Additionally, the nonhematopoietic function of NLRP12 to drive inflammation during colitis contributes to tumorigenesis more strongly than the hematopoietic function[77], and NLRP12 has intestinal epithelial cell-specific functions to suppress tumorigenesis[80]. These cell death-independent functions specifically in the intestine are likely dominant in NLRP12-deficient mice to drive the colitis severity. Collectively, our data suggest that the functions of NLRP12 and NLRC5 may complement each other in hemolytic models, with deletion of a single molecule being sufficient to provide protection. In contrast, in the colitis model, the presence of a rich microbial environment that releases multiple PAMPs and DAMPs may bypass this complementation, resulting in differing roles for the two proteins. In addition, recent biochemical data using an overexpression system suggest that human NLRP12 inhibits NLRP3-ASC complex formation[81], but studies in murine cells suggest NLRP12 and NLRP3 interact for inflammasome formation[82,83]; additional work is needed to understand the physiological relevance of these findings in primary cells and in humans.

Overall, our study identified NLRC5 as a critical NLR sensor that drives PANoptosis and pathology in multiple diseases. These findings suggest that targeting NLRC5 or other molecules in the NLRC5-NLRP12 cell death pathway may be therapeutically beneficial in the treatment of disease to reduce inflammation and improve patient outcomes.

Limitations of the study

This study demonstrates that NLRC5 is an important NLR sensor to drive PANoptosis and pathology in response to hemolytic triggers. While our immunoprecipitation data in both the endogenous and overexpression system suggest that NLRP12 is an integral component of the NLRC5-PANoptosome complex that drives cell death, the direct interactions of NLRC5, NLRP12, and other complex components require further characterization. Fully understanding this complex remains complicated by a lack of specific murine antibodies for NLRP12. This limitation also makes it difficult to determine the effects of NLRC5 on NLRP12 expression and functions in vivo, and further studies with new molecular tools will be needed to assess the interplay between these molecules. Furthermore, the use of nicotinamide as a modulator of NAD^+ levels provides critical insights into the role of NAD^+ levels in the NLRC5-mediated cell death pathway, but more precise reagents would be required to directly analyze the impact of NAD^+ levels in this process. Additionally, we demonstrated comparable $CD8^+$ T-cell infiltration in WT and NLRC5-deficient mice in the hemolytic disease model, but it remains possible that there is a role of MHC class I independent of its $CD8^+$ T cell regulatory function.

STAR METHODS

Resource Availability

Lead Contact—Further information and reasonable requests for reagents may be directed to, and will be fulfilled by, the lead contact Thirumala-Devi Kanneganti (thirumala-devi.kanneganti@stjude.org).

Materials Availability—All unique reagents generated in this study are available upon reasonable request from the Lead Contact.

Data and Code Availability

- The datasets generated and analyzed during the current study are contained within the manuscript and accompanying supplemental data figures and tables, and publicly available datasets analyzed can be found in the Gene Expression Omnibus database (GSE133181, GSE34404, GSE136046, GSE102881, GSE168532).
- This paper does not report original code.
- Any additional information required to reanalyze the data reported in this paper is available from the lead contact upon reasonable request.

Experimental Model and Study Participant Details

Mice—*Nlrp3*$^{-/-}$,[86] *Nlrp12*$^{-/-}$,[76] *Nlrc4*$^{-/-}$,[90] *Nlrc5*$^{-/-}$,[56] *Aim2*$^{-/-}$,[92] *Casp11*$^{-/-}$,[91] *Tlr2*$^{-/-}$,[87] *Tlr4*$^{-/-}$,[88] *Tlr2*$^{-/-}$*Tlr4*$^{-/-}$,[12] *Zbp1*$^{-/-}$,[89] *Casp1/11*$^{-/-}$*Casp8*$^{-/-}$*Ripk3*$^{-/-}$,[93] and *Casp8*$^{-/-}$*Ripk3*$^{-/-}$ mice[94] have been previously described. *Nlrc5*$^{-/-}$*Nlrp12*$^{-/-}$ mice were bred by crossing *Nlrc5*$^{-/-}$ (ref. [56]) with *Nlrp12*$^{-/-}$ (ref. [76]) mice. *Nlrc5*-KO^{line2} mice were generated at the Center for Advanced Genome Engineering (CAGE) at St. Jude Children's Research Hospital using CRISPR/Cas9 technology as described below. All mice were generated on or extensively backcrossed to the C57/BL6 background. Mice were bred at the Animal Resources Center at St. Jude Children's Research Hospital and maintained under specific pathogen-free conditions. Male and female 6- to 12-week-old mice were used for in vitro experiments in this study. Mice were maintained with a 12 h light/dark cycle and were fed standard chow. Animal studies were conducted under protocols approved by the St. Jude Children's Research Hospital committee on the Use and Care of Animals. For all in vivo experiments, male mice were housed with mixed bedding (bedding from all experimental cages was combined and re-distributed evenly across the cages) for 2 weeks before the beginning of the experimental treatment.

Generation of the Nlrc5-KO^{line2} mouse strain—The new *Nlrc5*$^{-/-}$ (*Nlrc5*-KO^{line2}) mouse was generated using CRISPR/Cas9 technology in collaboration with St. Jude's Center for Advanced Genome Engineering (CAGE) and the Transgenic/Gene Knockout Shared Resource facilities. Pronuclear-staged C57BL/6J zygotes were injected with Cas9 protein combined with an sgRNA targeting exon 4 (CAATGTTGTCGGCTGCTTCAggg, the pam sequence is underlined). The zygotes were surgically transplanted into the oviducts of pseudo-pregnant CD1 females, and newborn mice carrying a 56 bp deletion in exon 4

of the *Nlrc5* gene allele were identified by next generation sequencing (NGS) and Sanger sequencing methods and used to establish the *Nlrc5*-KO^{line2} colony. For routine genotyping, both the WT and mutant *Nlrc5* alleles were PCR amplified by using the primers NLRC5-GT_F1 (5'-GTATCAAGTGTGAGAGCTCCTAC-3'; primer P1) and NLRC5-GT_R1 (5'-CTCTGACTCTGGCATCAAGTAC −3'; primer P2) and subjected to Sangar sequencing (Figure S3B). The details of the generation of the CRISPR reagents were described previously[95]. The uniqueness of sgRNAs and the off-target sites with fewer than three mismatches were found using the Cas-OFFinder algorithm[96].

Methods Details

Bone marrow-derived macrophage (BMDM) generation—Primary mouse BMDMs from wild-type and indicated mutant mice were grown for 6 days in IMDM (12440053, Thermo Fisher Scientific) supplemented with 10% heat-inactivated fetal bovine serum (HI-FBS; S1620, Biowest), 30% L929 conditioned media, 1% non-essential amino acids (11140–050, Thermo Fisher Scientific), and 1% penicillin and streptomycin (15070–063, Thermo Fisher Scientific). BMDMs at a density of 1×10^6 cells/well in 12 well plates or 5×10^5 cells/well in 24 well plates were seeded into growth media overnight before use.

For experiments involving siRNA-mediated gene knockdown, the cells were resuspended in PBS at a cell density of 1×10^7 cells/ml, and 5 pmoles non-targeting (control) siRNA (D-001206-14-20, Horizon Discovery) or mouse-specific *Nlrc5* siRNA (M-067620-02-0005, Horizon Discovery) per million cells was used for transfection by electroporation (Neon Transfection System kit, MPK5000, Thermo Fisher Scientific). The cells were used for experiments 48 h after transfection.

Differentiation of human monocyte-derived macrophages and siRNA transfection—Fresh human blood was collected from the apheresis rings of anonymous healthy blood donors from the blood bank of St. Jude Children's Research Hospital, following a protocol reviewed and approved by the St. Jude IBC. Peripheral blood mononuclear cells (PBMCs) were isolated from the freshly collected blood using lymphoprep solution (cat. #07801/07811, Stemcell Technologies). Naive monocytes were purified from the PBMCs using monocyte isolation kit (EasySep direct human monocyte isolation kit, cat. #19669, Stemcell Technologies) strictly in accordance with the manufacturer's protocol. These purified monocytes were further differentiated into monocyte-derived macrophages by culturing in RPMI media (10-040-CV, Corning) supplemented with 10% HI-FBS, 1% penicillin-streptomycin, and 25 ng/ml human M-CSF (300–25, Peprotech) for 6 days in a CO_2 incubator supplied with 5% CO_2 in a humidified atmosphere. On day 2 and day 4, an additional 8–10 ml of media containing 25 ng/ml human M-CSF was added to the cells. On day 6, all the loosely attached and suspension cells were harvested and washed three times with PBS. The cells were resuspended in PBS at a cell density of 1×10^7 cells/ml. For siRNA-mediated knockdown of gene expression in monocyte-derived macrophages, 5 pmoles non-targeting (control) siRNA (D-001206-14-20, Horizon Discovery) or human specific *NLRC5* siRNA (M-018267-01-0005, Horizon Discovery) per million cells was used for transfection. Post-transfection, the cells were resuspended in RPMI medium supplemented with 10% HI-FBS, 1% penicillin-streptomycin,

and 25 ng/ml human M-CSF along with 1 ng/ml LPS and 20 ng/ml human IFN-γ (300–02, Peprotech) to polarize the cells to canonical macrophages. The cells were used for experiments 48 h after transfection.

Cell stimulation—BMDMs were treated in DMEM (11995–065, Gibco) containing 10% HI-FBS and 1% penicillin and streptomycin with the following DAMPs, PAMPs, cytokines, and inhibitors alone or in combinations where indicated: 50 μM Hemin (heme; H9039, Sigma), 15 ng/mL ultrapure LPS from *E. coli* (0111: B4) (tlrl-3pelps, InvivoGen), 500 ng/mL Pam3CSK4 (Pam3; tlrl-pms, InvivoGen), 500 ng/mL R848 (tlrl-r848, InvivoGen), 1 μg/mL poly(I:C) (tlrl-picw, InvivoGen), 100 ng/mL TNF (Peprotech, 315-01A), 2 μM MCC950 (inh-mcc, Invivogen), 5 mM N-acetyl L-cysteine (NAC) (A9165, Sigma-Aldrich), and 5 mM or 10 mM nicotinamide (NAM) (N3376, Sigma-Aldrich). Hemin (100 mM stock) was prepared by dissolving in filter sterilized 0.1 M NaOH and neutralizing (to pH 7.2) with 1 M HCl, as previously described[97]. Stocks were freshly prepared before the experiment. For LPS plus ATP stimulation, BMDMs were primed for 4 h with 100 ng/ml ultrapure LPS and then stimulated with 5 mM ATP (101275310001, Roche). For DNA transfection, each reaction consisted of 2 μg poly(dA:dT) (tlrl-patn, InvivoGen) resuspended in PBS and mixed with 0.6 μl Xfect polymer in Xfect reaction buffer (631318, Clontech Laboratories, Inc). After 10 min, DNA complexes were added to BMDMs in Opti-MEM (31985–070, Thermo Fisher Scientific). For LPS transfection, the BMDMs were primed for 4 h with 100 ng/ml ultrapure LPS and then transfected with 2 μg of LPS per well following the same steps used for DNA transfection.

Virus and bacteria culture—IAV (A/Puerto Rico/8/34, H1N1 [PR8]) was prepared as previously described[98] and propagated from 11-day-old embryonated chicken eggs by allantoic inoculation. IAV titer was measured by plaque assay in Madin–Darby canine kidney cells (CCL-34, ATCC). *Salmonella enterica* serovar Typhimurium (*Salmonella*) strain SL1344 and *E. coli* (11775, ATCC) were inoculated into Luria–Bertani media (3002–031, MP Biomedicals) and incubated overnight under aerobic conditions at 37°C. *S.* Typhimurium SL1344 was subcultured (1:10) into fresh LB media for 3 h at 37°C to generate log phase grown bacteria. For virus infection, IAV (multiplicity of infection [MOI] 20) was used in serum-free media; 1 h after infection, 10% HI-FBS was added to the cells. For bacterial infection, *S.* Typhimurium (MOI 1) and *E. coli* (MOI 20) were used. Four hours after infection, *E. coli*-infected cells were washed two times with PBS, and 50 μg/ml gentamicin (15750–060, Thermo Fisher Scientific) was added to kill extracellular bacteria.

Real-time imaging for cell death—The kinetics of cell death were monitored using the IncuCyte S3 or SX5 (Sartorius) live-cell analysis system. BMDMs were seeded in 24-well tissue culture plates and treated with the indicated stimuli. Cell death was measured by propidium iodide (PI; P3566, Life Technologies) incorporation following the manufacturer's protocol. The plate was scanned for the indicated time durations, with fluorescent and phase-contrast images acquired in real-time every 1 h. PI-positive dead cells are marked with a red mask and were quantified using the software package supplied with the IncuCyte imager.

Detection of cellular ROS—Cellular ROS was detected by staining the cells with CellROX™ Deep Red Reagent (C10422, invitrogen), and the generation of ROS was monitored using the IncuCyte live-cell analysis system. Briefly, BMDMs were washed once with PBS, and cells were treated with heme plus Pam3 in the presence of 1.25 μM CellROX reagent. The images were then acquired using the IncuCyte system.

Immunoblot analysis—After appropriate treatments, cells were lysed along with culture supernatants in caspase lysis buffer (containing 10% NP-40, 25 mM DTT and 1× protease and phosphatase inhibitors (11697498001 and 04906837001, respectively, Roche)) and SDS sample loading buffer (with 2-mercaptoethanol) for probing caspase activation. For immunoblot assessment of signaling activation, culture supernatants were removed, cells were washed once with 1× Dulbecco's PBS (DPBS; 14190–250, Thermo Fisher Scientific) and lysed in RIPA buffer and SDS sample loading buffer. Proteins were resolved on 8–12% polyacrylamide gels and transferred onto PVDF membranes (IPVH00010, Millipore) using the Trans-Blot® Turbo™ system. After blocking non-specific binding with 5% skim milk, membranes were incubated overnight with the following primary antibodies against: caspase-1 (AG-20B-0044, AdipoGen, 1:1000), caspase-3 (#9662, Cell Signaling Technology [CST], 1:1000), cleaved caspase-3 (#9661, CST, 1:1000), caspase-7 (#9492, CST, 1:1000), cleaved caspase-7 (#9491, CST, 1:1000), caspase-8 (#4927, CST, 1:1000), cleaved caspase-8 (#8592, CST, 1:1000), p-MLKL (#37333, CST, 1:1000), t-MLKL (AP14272B, Abgent, 1:1000), GSDMD (ab209845, Abcam, 1:1000), GSDME (ab215191, Abcam, 1:1000), Myc (#2276, CST, 1:1000), NLRP3 (#AG-20B-0014, AdipoGen, 1:1000), NLRC5 (clone E1E9Y; #72379, CST, 1:2000), FLAG (#F1804, Sigma, 1:1000), HA (#2367, CST, 1:1000), human caspase-8 (#ALX-804-242, Enzo Life Science, 1:1000), LCN2 (ab216462, Abcam, 1:2000), α-Tubulin (#2144, CST, 1:1000), GAPDH (sc-166574 HRP, Santa Cruz, 1:5000), and β-actin (sc-47778 HRP, Santa Cruz, 1:5000). Membranes were then washed and probed with the appropriate horseradish peroxidase (HRP)-conjugated secondary antibodies (anti-mouse [315-035-047] and anti-rabbit [111-035-047], 1:5000, Jackson ImmunoResearch Laboratories). Immunoblot images were acquired on an Amersham Imager using Immobilon® Forte Western HRP Substrate (WBLUF0500, Millipore) or SuperSignal™ West Femto Maximum Sensitivity Substrate (34096, Thermo Fisher Scientific). For quantification, densitometric measurements of the target proteins were performed using ImageJ software (version 1.53k, NIH), and the measurements were normalized to the appropriate loading control.

IL-1β measurement—IL-1β released into the cultured supernatant was measured using ELISA for IL-1β (88-7013-88, Invitrogen) following the manufacturer's instructions.

Microarray and RNA-seq analysis—Gene expression analysis was performed as described previously[12]. Briefly, four datasets deposited in GEO (accession IDs: GSE34404[21], GSE136046[20], GSE102881[22], GSE168532[22,23] were used to estimate the role of NLRs in datasets relevant for hemolytic diseases. GSE34404[21] compares whole blood RNA-seq profiles of 155 West-African children, including 94 cases of symptomatic *Plasmodium falciparum* infection and 61 age-matched controls. GSE136046[20] consists of expression profiles of affinity purified $CD71^+$ cells from three patients with *Plasmodium*

vivax at day 1 (diagnosis visit) and day 42 after curative drug treatment (convalescence visit). From GSE102881[22], RNA-seq profiles were obtained from $CD34^+$ hematopoietic stem/progenitor cells (HSPCs) collected from the bone marrow of two healthy donors and two patients with sickle cell disease (SCD). GSE168532[22,23] consists of transcriptomic profiles of classical monocytes from the peripheral blood of six healthy controls and 13 patients with SCD.

For each of these datasets, quality control steps were performed as described previously[12]. Differential expression analysis was performed using the limma v3.52.1[99] package in R v4.1.1. The Benjamini-Hochberg[100] adjusted P value < 0.05 for GSE34404 and GSE168532 was used to determine the set of differentially expressed genes. However, owing to the small sample sizes for GSE136046 (three cases and three controls) and GSE102881 (two cases and two controls), P value adjustments were not made for these three datasets. A P value < 0.05 was used to estimate the set of differentially expressed genes for GSE136046 and GSE102881. The NLRs were assessed to determine which were overexpressed across the disease-relevant datasets and then sorted based on their average fold-change across these datasets. The results were visualized using Heatmap from the Complex Heatmap v2.8.0[101] package.

Immunofluorescence staining and confocal microscopy—BMDMs were seeded onto poly-D-lysine coated coverslips in 24-well plates at a density of 0.5×10^6 cells/well. The simulations were performed as indicated and described above. Cells were then washed with PBS once and fixed for 10 min at 4°C in ice-chilled 99.8% methanol (A412-4, Fisher). Cells were then washed with PBS three times (10 min each) and permeabilized and blocked by incubating in permeabilization and blocking buffer (PBS containing 10% normal goat serum (#5425, CST), 1% bovine serum albumin (A-421-10, GoldBio), and 0.5% Triton X-100 (T8787, Sigma)) for 1 h at room temperature. Cells were then incubated with the following primary antibodies overnight (16 h) at 4°C: mouse anti-ASC (clone 2EI-7, #04–147, Millipore, 1:100), rat anti-mRIPK3 (clone 8G7, #MABC1595, Millipore, 1:200), and rabbit anti-NLRC5 (clone E1E9Y, #72379, CST, 1:500) in permeabilization and blocking buffer. Cells were then washed with PBS three times (10 min each) and stained with secondary antibodies for 1 h at room temperature in the dark. The secondary antibodies used were goat anti-mouse IgG AlexaPlus-488 (#A32723, Thermo Fisher Scientific), goat anti-rat IgG Alexa-568 (#A11077, Thermo Fisher Scientific), and goat anti-rabbit IgG Alexa Fluor-633 (#A-21070, Thermo Fisher Scientific). All secondary antibodies were diluted at 1:500 in permeabilization and blocking buffer. After secondary antibody staining, cells were washed with PBS three times (10 min each). Cells were then fixed again for 10 min in 2% PFA and then washed with PBS three times (5 min each). Cells were then blocked in rat-IgG Isotype control (#02–9602, Thermo Fisher Scientific) at 1 μg/ml in permeabilization and blocking buffer for 30 min. Cells were then washed with PBS three times (10 min each), and then stained with Alexa Fluor 594-directly conjugated anti-caspase-8 antibody at 1:200 in permeabilization and blocking buffer at 4°C overnight protected from light. Alexa Fluor 594 Antibody Labeling Kit, (#A20185, Thermo Fisher Scientific) was used for conjugation of anti-caspase-8 (clone 3B10, #AG-20T-0138-C100, AdipoGen). Cells were then washed with PBS three times (10 min each) and then counterstained with 1 μg/mL DAPI for 5

min, washed once with PBS, and mounted using Pro-Long™ Diamond Antifade Mountant (#P36961, Invitrogen) on glass slides.

Coverslips were imaged at 48 h post-mounting using a Leica SP8 laser scanning confocal microscope using 512 × 512 pixels, scan speed 400 Hz, and zoom factor 1 with a 63 × 1.4 NA oil objective. The laser lines used were 405 nm (diode), 488 nm, 568 nm, 594 nm, and 633 nm (white light laser). Images were analyzed manually using Leica LAS X software.

Overexpression and immunoprecipitation—For immunoprecipitation in the overexpression system, HEK293T cells (CRL-3216, ATCC) were seeded into six-well plates and transfected with a combined total of 5 ug of the following plasmids (1:1:1:1:1, molar ratio): pcDNA3-Myc-h*ASC* (#73952, Addgene), pcDNA3-h*CASP8* (#11817, Addgene), pcDNA3-HA-h*RIPK3* (#78804, Addgene), pcDNA3-Myc-h*NLRC5* (#37509, Addgene), and pcDNA3-h*NLRP12*-FLAG (Human *NLRP12* PCR product amplified using cDNA and cloned in pcDNA™3.1 (+) Mammalian Expression Vector (#V790-20, Thermo Fisher Scientific), with or without an equimolar ratio of pEGFP-C2-h*NLRP3* (#73955, Addgene), and incubated for 24–36 h. Immunoprecipitation was performed as previously described[12,102] with minor modifications. Briefly, cells were collected and lysed in an ice-cold lysis buffer containing 20 mM Tris-HCl (pH 7.4), 150 mM NaCl, 1% Triton X-100, 10% glycerol, 1 mM Na_3VO_4, 2 mM PMSF, EDTA-free protease inhibitor cocktail (#A32965, Thermo Fisher Scientific), phosphatase inhibitor cocktail (#4906845001, Sigma), and 25 μM Z-VAD-FMK (#S7023, Selleckchem). After centrifugation at 16,000 × g for 10 min, the lysates were incubated with either IgG control antibody (#3900S, CST), anti-ASC antibody (#AG-25B-0006, AdipoGen), anti-human NLRP12 antibody (#AP14014a, Abcepta), or anti-HA (#3724S, CST; to detect RIPK3-HA) overnight at 4°C. The immunoprecipitated proteins were then added to washed Protein A/G magnetic beads (#88802, Thermo Fisher Scientific) and incubated for 2 h at 4°C. Subsequently, the beads were washed 4 times with lysis buffer and boiled in 2× SDS loading buffer at 100○C for 5 min. Immunoprecipitates in sample buffer were subjected to immunoblotting analysis with 0.5% of input sample and 12% of pull-down sample per lane. After blocking non-specific binding with 5% skim milk, membranes were incubated overnight with the following primary antibodies against: Myc (#2276, CST, 1:1000), NLRP3 (#AG-20B-001, AdipoGen, 1:1000), FLAG (#F1804, Sigma, 1:1000), HA (#2367, CST, 1:1000), human caspase-8 (#ALX-804-242, Enzo Life Science, 1:1000), and GAPDH-HRP (#166574, Santa Cruz, 1:5000).

For endogenous immunoprecipitation, 3×10^7 BMDMs were seeded and stimulated with heme plus Pam3 for 28 h. The BMDMs were then washed with ice cold PBS and scraped from the plate to collect in PBS. The cell pellet was then gently resuspended in 300 μl ice-cold lysis buffer (as described above) and incubated on a rocker at 4°C for 1 h. After centrifugation at 14,000 × g for 10 min, the lysates were incubated with either IgG control antibody (#3900S, CST) or anti-ASC antibody (#AG-25B-006, AdipoGen) overnight at 4°C. Washed Protein A/G magnetic beads were added and incubated for 2 h at 4°C. Subsequently, the beads were washed 5 times with lysis buffer and boiled in 2× SDS loading buffer at 100○C for 5 min. Immunoprecipitates in sample buffer were subjected to immunoblotting analysis with 0.5% of input sample and 12% of pull-down sample per lane. After blocking

non-specific binding with 5% skim milk, membranes were incubated overnight with the following primary antibodies against: ASC (#AG-25B-006, AdipoGen, 1:1000), RIPK3 (#2283, Prosci, 1:1000), caspase-8 (#AG-20T-0138-C100, AdipoGen, 1:1000), NLRP3 (#AG-20B-0014, AdipoGen, 1:1000), and NLRC5 (#72379, CST, 1:2000).

For both overexpression and endogenous IPs, membranes were then washed and probed with the appropriate horseradish peroxidase (HRP)–conjugated secondary antibodies (anti-mouse [#315-035-047] and anti-rabbit [#111-035-047], Jackson ImmunoResearch Laboratories). Immunoblot images were acquired on an Amersham Imager using Immobilon® Forte Western HRP Substrate or SuperSignal™ West Femto Maximum Sensitivity Substrate.

In vivo models—Male age-matched 8- to 10-week-old male WT and *Nlrc5*$^{-/-}$ (ref. [56]) mice were used for in vivo analyses. For all in vivo experiments, mice were housed with mixed bedding (bedding from all experimental cages was combined and re-distributed evenly across the cages) for 2 weeks before the beginning of the experimental treatment.

A hemolytic inflammatory disease model was induced as described previously[12]. Briefly, LPS, 1 μg/g body weight (L2630, Sigma), and phenylhydrazine, 0.125 mg/g body weight (114715, Sigma), were used. Briefly, LPS was dissolved in sterile DPBS, aliquoted and stored in −80°C until used. Phenylhydrazine was weighed and dissolved in sterile DPBS; then the pH was adjusted to 7.4 using 2 M NaOH, and phenylhydrazine was filtered through a 0.22 μm syringe filter (SLGPR33RS, Millipore). Indicated genotypes were injected intraperitoneally with LPS and phenylhydrazine, where LPS was added to sterile, filtered phenylhydrazine and mixed before injection.

An acute colitis model was induced using dextran sodium sulfate (DSS) as described previously[45], with minor modifications. Briefly, mice were dosed with 4.5% DSS in the drinking water for 6 days, followed by regular drinking water until the end of the experiment (day 7).

A model of hemophagocytic lymphohistiocytosis (HLH) was induced by sequential challenge of poly I:C and LPS as described previously[49], with minor modifications. Mice were injected intraperitoneally with 5 mg/kg body weight of high molecular weight poly I:C (InvivoGen, tlrlpic). After 24 h following poly(I:C) injection, mice were challenged with a sublethal dose of LPS (2.5 mg/kg body weight). Mice were monitored for survival.

During in vivo studies, all mice are monitored for grooming and normal gait. If a mouse has very rough or scruffy hair or is moribund, it has reached a humane endpoint and is euthanized. Additionally, all mice are monitored for body weight, and if a mouse loses > 20% of its body weight, it has reached a humane endpoint and is euthanized. Additionally, any mouse that exhibits paralysis, is cold to the touch, has dyspnea, or loses its righting reflex has reached a humane endpoint and is euthanized.

Histopathology—Kidneys from WT and *Nlrc5*$^{-/-}$ mice in the phenylhydrazine and LPS model and colons from WT and *Nlrc5*$^{-/-}$ mice in the DSS model were fixed in 10% formalin, then processed and embedded in paraffin by standard procedures. Sections (5 μM) were stained with hematoxylin and eosin (H&E) and examined by a pathologist blinded to

the experimental groups. Scoring criteria: 0 = absent; 1 = rare, minimal; 2 = scattered mild; 3 = multifocal, moderate; 4 = extensive, marked; 5 = severe.

For all other immunohistochemistry, tissues were fixed by immersion in 10% neutral buffered formalin (NBF) for at least 72 h and then embedded in paraffin, sectioned at 4 μm, mounted on positively charged glass slides (Superfrost Plus; Thermo Fisher Scientific), and dried at 60°C for 20 min. For detection of LCN2 and CD8 in fixed tissues, sections were subjected to antigen retrieval at 100°C for 32 min in Cell conditioning 1 (CC1) Buffer (#950–500; Roche Diagnostics, Indianapolis, IN) on a Discovery Ultra immunostainer (Ventana Medical Systems). Rat monoclonal primary antibodies to LCN2 at 1:500 (#NBP1-05183; Novus Biologicals) or mouse CD8 at 1:200 (#14-0808-82; eBioscience) were applied for 60 min at 37°C. For detection, a secondary peroxidase (HRP)-conjugated anti-rat IgG antibody (#760–4457, Roche Diagnostics) was applied for 16 min at room temperature and then developed with ChromoMap DAB (3,3′- diaminobenzidine tetrahydrochloride) chromogen and counterstained with hematoxylin (all from Roche Diagnostics).

Colitis scores were assigned based on inflammation, ulceration, hyperplasia, and the extent or severity of the damage. Severity scores for inflammation were assigned as follows: 0 = normal (within normal limits); 2 = minimal (mixed inflammation, small, focal, or widely separated, limited to lamina propria); 15 = mild (multifocal mixed inflammation, often extending into submucosa); 40 = moderate (large multifocal lesions within mixed inflammation involving mucosa and submucosa); 80 = marked (extensive mixed inflammation with edema and erosions); 100 = severe (diffuse inflammation with transmural lesions and multiple ulcers). Scores for ulceration were assigned as follows: 0 = normal (none); 2 = minimal (only one small focus of ulceration involving fewer than 5 crypts); 15 = mild (a few small ulcers, up to 5 crypts); 40 = moderate (multifocal ulcers, up to 10 crypts); 80 = marked (multifocal to coalescing ulcers involving more than 10 crypts each); 100 = severe (extensive to diffuse with multiple ulcers covering more than 20 crypts each). Scores for hyperplasia were assigned as follows: 0 = normal; 2 = minimal (some areas with crypts elongated and increased mitoses); 15 = mild (multifocal areas with crypts elongated up to twice the normal thickness, normal goblet cells present); 40 = moderate (extensive areas with crypts up to 2 times normal thickness, reduced goblet cells); 80 = marked (mucosa over twice the normal thickness, hyperchromatic epithelium, reduced or rare goblet cells, possibly foci of arborization); 100 = severe (mucosa twice the normal thickness, marked hyperchromasia, crowding/stacking, absence of goblet cells, high mitotic index and arborization). Scores of extent were assigned as follows: 0 = normal (rare or inconspicuous lesions); 2 = minimal (less than 5% involvement); 15 = mild (multifocal but conspicuous lesions, 5 to 10% involvement); 40 = moderate (multifocal, prominent lesions, 10 to 50% involvement); 80 = marked (coalescing to extensive lesions or areas of inflammation with some loss of structure, 50 to 90% involvement); 100 = severe (diffuse lesion with effacement of normal structure, > 90% involvement).

For image analysis, slides were scanned, and the percentage area of renal parenchyma that was labeled for LCN2 was determined by quantitative morphometry using the HALO™ Area Quantification v2.4.3 algorithm (IndicaLabs). Similarly, the numbers of $CD8^+$ T cells in the

kidney were determined using the HALO™ Multiplex IHC v3.4.9 algorithm (IndicaLabs). In this iterative process, a pathologist annotated training regions and, after visually confirming the accuracy of results in additional sections, adjusted program settings until positive signal was consistently correctly annotated. To further improve the AI recognition accuracy, training cycles were repeated until the number of misrecognized regions was reduced to an acceptable level (i.e. until the analysis results did not change appreciably with the completion of further training).

Clinical chemistry analysis—Serum creatinine (A11A01933), BUN (A11A01641), iron (A11A01637), ALT (A11A01627), and AST (A11A01629) were detected using ABX Pentra 400 Reagents (HORIBA) and hemoglobin was detected using VetHemaChemRx (Oxford science) according to the manufacturer's instructions.

Statistical analysis—GraphPad Prism 9.0 and 10.0 software were used for in vitro and murine in vivo data analysis. Data are shown as mean ± SEM. Statistical significance was determined by unpaired t tests for two groups, one- or two-way ANOVA (with Dunnett's or Tukey's multiple comparisons tests) for three or more groups, or log-rank (Mantel-Cox) test for survival analysis. P value < 0.05 was considered statistically significant.

Supplementary Material

Refer to Web version on PubMed Central for supplementary material.

ACKNOWLEDGEMENTS

We thank all the members of the Kanneganti laboratory for their comments and suggestions during the development of this manuscript, and particularly R.K.S. Malireddi, PhD, B.R. Sharma, PhD, V. Nadella, PhD, and K. Thorne for their technical assistance. Work from our laboratory is supported by the US National Institutes of Health (AI101935, AI124346, AI160179, AR056296, and CA253095 to T.-D.K.) and the American Lebanese Syrian Associated Charities (to T.-D.K.). The content is solely the responsibility of the authors and does not necessarily represent the official views of the National Institutes of Health. We thank V.M. Dixit and N. Kayagaki (Genentech) for the *Casp11*$^{-/-}$ mutant mouse strain, and we thank S. Akira for generously supplying the *Nlrc5*$^{-/-}$ mice.

REFERENCES

1. Kanneganti TD (2020). Intracellular innate immune receptors: Life inside the cell. Immunol Rev 297, 5–12. 10.1111/imr.12912. [PubMed: 32856334]
2. Harton JA, Linhoff MW, Zhang J, and Ting JP (2002). Cutting edge: CATERPILLER: a large family of mammalian genes containing CARD, pyrin, nucleotide-binding, and leucine-rich repeat domains. J Immunol 169, 4088–4093. [PubMed: 12370334]
3. Inohara N, and Nuñez G (2003). NODs: intracellular proteins involved in inflammation and apoptosis. Nat Rev Immunol 3, 371–382. 10.1038/nri1086. [PubMed: 12766759]
4. Kobayashi KS, and van den Elsen PJ (2012). NLRC5: a key regulator of MHC class I-dependent immune responses. Nat Rev Immunol 12, 813–820. 10.1038/nri3339. [PubMed: 23175229]
5. Meissner TB, Li A, Biswas A, Lee KH, Liu YJ, Bayir E, Iliopoulos D, van den Elsen PJ, and Kobayashi KS (2010). NLR family member NLRC5 is a transcriptional regulator of MHC class I genes. Proc Natl Acad Sci U S A 107, 13794–13799. 10.1073/pnas.1008684107. [PubMed: 20639463]
6. Yoshihama S, Roszik J, Downs I, Meissner TB, Vijayan S, Chapuy B, Sidiq T, Shipp MA, Lizee GA, and Kobayashi KS (2016). NLRC5/MHC class I transactivator is a target for immune

evasion in cancer. Proc Natl Acad Sci U S A 113, 5999–6004. 10.1073/pnas.1602069113. [PubMed: 27162338]

7. Zupin L, Navarra CO, Robino A, Bevilacqua L, Di Lenarda R, Gasparini P, and Crovella S (2017). NLRC5 polymorphism is associated with susceptibility to chronic periodontitis. Immunobiology 222, 704–708. 10.1016/j.imbio.2017.01.001. [PubMed: 28122660]
8. Zhong J, Liu L, Lu Y, Gu Y, Zhao J, Chen B, Zhou W, and Su X (2022). NLRP3, NLRC4 and NLRC5 Gene Polymorphisms Associate with Susceptibility of Pulmonary Aspergillosis in Non-Neutropenic Patients. J Clin Med 11. 10.3390/jcm11071870.
9. Davis BK, Roberts RA, Huang MT, Willingham SB, Conti BJ, Brickey WJ, Barker BR, Kwan M, Taxman DJ, Accavitti-Loper MA, et al. (2011). Cutting edge: NLRC5-dependent activation of the inflammasome. J Immunol 186, 1333–1337. 10.4049/jimmunol.1003111. [PubMed: 21191067]
10. Cui J, Zhu L, Xia X, Wang HY, Legras X, Hong J, Ji J, Shen P, Zheng S, Chen ZJ, and Wang RF (2010). NLRC5 negatively regulates the NF-kappaB and type I interferon signaling pathways. Cell 141, 483–496. 10.1016/j.cell.2010.03.040. [PubMed: 20434986]
11. Wu CH, Abd-El-Haliem A, Bozkurt TO, Belhaj K, Terauchi R, Vossen JH, and Kamoun S (2017). NLR network mediates immunity to diverse plant pathogens. Proc Natl Acad Sci U S A 114, 8113–8118. 10.1073/pnas.1702041114. [PubMed: 28698366]
12. Sundaram B, Pandian N, Mall R, Wang Y, Sarkar R, Kim HJ, Malireddi RKS, Karki R, Janke LJ, Vogel P, and Kanneganti TD (2023). NLRP12-PANoptosome activates PANoptosis and pathology in response to heme and PAMPs. Cell 186, 2783–2801 e2720. 10.1016/j.cell.2023.05.005. [PubMed: 37267949]
13. Gozzelino R, Jeney V, and Soares MP (2010). Mechanisms of cell protection by heme oxygenase-1. Annu Rev Pharmacol Toxicol 50, 323–354. 10.1146/annurev.pharmtox.010909.105600. [PubMed: 20055707]
14. Martins R, and Knapp S (2018). Heme and hemolysis in innate immunity: adding insult to injury. Curr Opin Immunol 50, 14–20. 10.1016/j.coi.2017.10.005. [PubMed: 29107115]
15. Soares MP, and Bozza MT (2016). Red alert: labile heme is an alarmin. Curr Opin Immunol 38, 94–100. 10.1016/j.coi.2015.11.006. [PubMed: 26741528]
16. Fortes GB, Alves LS, de Oliveira R, Dutra FF, Rodrigues D, Fernandez PL, Souto-Padron T, De Rosa MJ, Kelliher M, Golenbock D, et al. (2012). Heme induces programmed necrosis on macrophages through autocrine TNF and ROS production. Blood 119, 2368–2375. 10.1182/blood-2011-08-375303. [PubMed: 22262768]
17. Seixas E, Gozzelino R, Chora A, Ferreira A, Silva G, Larsen R, Rebelo S, Penido C, Smith NR, Coutinho A, and Soares MP (2009). Heme oxygenase-1 affords protection against noncerebral forms of severe malaria. Proc Natl Acad Sci U S A 106, 15837–15842. 10.1073/pnas.0903419106. [PubMed: 19706490]
18. Coll RC, Robertson AA, Chae JJ, Higgins SC, Munoz-Planillo R, Inserra MC, Vetter I, Dungan LS, Monks BG, Stutz A, et al. (2015). A small-molecule inhibitor of the NLRP3 inflammasome for the treatment of inflammatory diseases. Nat Med 21, 248–255. 10.1038/nm.3806. [PubMed: 25686105]
19. Chen KW, Demarco B, Heilig R, Shkarina K, Boettcher A, Farady CJ, Pelczar P, and Broz P (2019). Extrinsic and intrinsic apoptosis activate pannexin-1 to drive NLRP3 inflammasome assembly. The EMBO journal 38. 10.15252/embj.2019101638.
20. Brito MAM, Baro B, Raiol TC, Ayllon-Hermida A, Safe IP, Deroost K, Figueiredo EFG, Costa AG, Armengol MDP, Sumoy L, et al. (2022). Morphological and Transcriptional Changes in Human Bone Marrow During Natural Plasmodium vivax Malaria Infections. J Infect Dis 225, 1274–1283. 10.1093/infdis/jiaa177. [PubMed: 32556188]
21. Idaghdour Y, Quinlan J, Goulet J-P, Berghout J, Gbeha E, Bruat V, de Malliard T, Grenier J-C, Gomez S, Gros P, et al. (2012). Evidence for additive and interaction effects of host genotype and infection in malaria. Proc. Natl. Acad. Sci. U. S. A. 109, 16786–16793. 10.1073/pnas.1204945109. [PubMed: 22949651]
22. Lagresle-Peyrou C, Lefrère F, Magrin E, Ribeil J-A, Romano O, Weber L, Magnani A, Sadek H, Plantier C, Gabrion A, et al. (2018). Plerixafor enables safe, rapid, efficient mobilization of

hematopoietic stem cells in sickle cell disease patients after exchange transfusion. Haematologica 103, 778–786. 10.3324/haematol.2017.184788. [PubMed: 29472357]

23. Liu Y, Pal M, Bao W, Shi PA, Lobo CA, An X, Manwani D, Zhong H, and Yazdanbakhsh K (2021). Type I interferon is induced by hemolysis and drives antibody-mediated erythrophagocytosis in sickle cell disease. Blood 138, 1162–1171. 10.1182/blood.2021011629. [PubMed: 34166491]
24. Figueiredo RT, Fernandez PL, Mourao-Sa DS, Porto BN, Dutra FF, Alves LS, Oliveira MF, Oliveira PL, Graca-Souza AV, and Bozza MT (2007). Characterization of heme as activator of Toll-like receptor 4. J Biol Chem 282, 20221–20229. 10.1074/jbc.M610737200. [PubMed: 17502383]
25. Aliprantis AO, Yang RB, Mark MR, Suggett S, Devaux B, Radolf JD, Klimpel GR, Godowski P, and Zychlinsky A (1999). Cell activation and apoptosis by bacterial lipoproteins through toll-like receptor-2. Science 285, 736–739. 10.1126/science.285.5428.736. [PubMed: 10426996]
26. Brightbill HD, Libraty DH, Krutzik SR, Yang RB, Belisle JT, Bleharski JR, Maitland M, Norgard MV, Plevy SE, Smale ST, et al. (1999). Host defense mechanisms triggered by microbial lipoproteins through toll-like receptors. Science 285, 732–736. 10.1126/science.285.5428.732. [PubMed: 10426995]
27. Murphy MP (2009). How mitochondria produce reactive oxygen species. Biochem J 417, 1–13. 10.1042/BJ20081386. [PubMed: 19061483]
28. Yang H, Yang T, Baur JA, Perez E, Matsui T, Carmona JJ, Lamming DW, Souza-Pinto NC, Bohr VA, Rosenzweig A, et al. (2007). Nutrient-sensitive mitochondrial NAD+ levels dictate cell survival. Cell 130, 1095–1107. 10.1016/j.cell.2007.07.035. [PubMed: 17889652]
29. Du L, Zhang X, Han YY, Burke NA, Kochanek PM, Watkins SC, Graham SH, Carcillo JA, Szabo C, and Clark RS (2003). Intra-mitochondrial poly(ADP-ribosylation) contributes to NAD+ depletion and cell death induced by oxidative stress. J Biol Chem 278, 18426–18433. 10.1074/jbc.M301295200. [PubMed: 12626504]
30. Sun C, Seranova E, Cohen MA, Chipara M, Roberts J, Astuti D, Palhegyi AM, Acharjee A, Sedlackova L, Kataura T, et al. (2023). NAD depletion mediates cytotoxicity in human neurons with autophagy deficiency. Cell Rep 42, 112372. 10.1016/j.celrep.2023.112372. [PubMed: 37086404]
31. Pajuelo D, Gonzalez-Juarbe N, Tak U, Sun J, Orihuela CJ, and Niederweis M (2018). NAD(+) Depletion Triggers Macrophage Necroptosis, a Cell Death Pathway Exploited by Mycobacterium tuberculosis. Cell Rep 24, 429–440. 10.1016/j.celrep.2018.06.042. [PubMed: 29996103]
32. Covarrubias AJ, Kale A, Perrone R, Lopez-Dominguez JA, Pisco AO, Kasler HG, Schmidt MS, Heckenbach I, Kwok R, Wiley CD, et al. (2020). Senescent cells promote tissue NAD(+) decline during ageing via the activation of CD38(+) macrophages. Nat Metab 2, 1265–1283. 10.1038/s42255-020-00305-3. [PubMed: 33199924]
33. Cameron AM, Castoldi A, Sanin DE, Flachsmann LJ, Field CS, Puleston DJ, Kyle RL, Patterson AE, Hassler F, Buescher JM, et al. (2019). Inflammatory macrophage dependence on NAD(+) salvage is a consequence of reactive oxygen species-mediated DNA damage. Nat Immunol 20, 420–432. 10.1038/s41590-019-0336-y. [PubMed: 30858618]
34. Wan L, Essuman K, Anderson RG, Sasaki Y, Monteiro F, Chung EH, Osborne Nishimura E, DiAntonio A, Milbrandt J, Dangl JL, and Nishimura MT (2019). TIR domains of plant immune receptors are NAD(+)-cleaving enzymes that promote cell death. Science 365, 799–803. 10.1126/science.aax1771. [PubMed: 31439793]
35. Essuman K, Summers DW, Sasaki Y, Mao X, Yim AKY, DiAntonio A, and Milbrandt J (2018). TIR Domain Proteins Are an Ancient Family of NAD(+)-Consuming Enzymes. Curr Biol 28, 421–430 e424. 10.1016/j.cub.2017.12.024. [PubMed: 29395922]
36. Liu G, Foster J, Manlapaz-Ramos P, and Olivera BM (1982). Nucleoside salvage pathway for NAD biosynthesis in Salmonella typhimurium. J Bacteriol 152, 1111–1116. 10.1128/jb.152.3.1111-1116.1982. [PubMed: 6216244]
37. Kang HT, Lee HI, and Hwang ES (2006). Nicotinamide extends replicative lifespan of human cells. Aging Cell 5, 423–436. 10.1111/j.1474-9726.2006.00234.x. [PubMed: 16939485]

38. Kang HT, and Hwang ES (2009). Nicotinamide enhances mitochondria quality through autophagy activation in human cells. Aging Cell 8, 426–438. 10.1111/j.1474-9726.2009.00487.x. [PubMed: 19473119]
39. Beutler E (1969). Drug-induced hemolytic anemia. Pharmacol Rev 21, 73–103. [PubMed: 4887725]
40. Li Q, Wang Z, Zhang Y, Zhu J, Li L, Wang X, Cui X, Sun Y, Tang W, Gao C, et al. (2018). NLRC5 deficiency protects against acute kidney injury in mice by mediating carcinoembryonic antigen-related cell adhesion molecule 1 signaling. Kidney Int 94, 551–566. 10.1016/j.kint.2018.02.031. [PubMed: 29907459]
41. Luan P, Zhuang J, Zou J, Li H, Shuai P, Xu X, Zhao Y, Kou W, Ji S, Peng A, et al. (2018). NLRC5 deficiency ameliorates diabetic nephropathy through alleviating inflammation. FASEB J 32, 1070–1084. 10.1096/fj.201700511RR. [PubMed: 29070585]
42. Viau A, El Karoui K, Laouari D, Burtin M, Nguyen C, Mori K, Pillebout E, Berger T, Mak TW, Knebelmann B, et al. (2010). Lipocalin 2 is essential for chronic kidney disease progression in mice and humans. J Clin Invest 120, 4065–4076. 10.1172/JCI42004. [PubMed: 20921623]
43. Xu K, Shang N, Levitman A, Corker A, Kudose S, Yaeh A, Neupane U, Stevens J, Sampogna R, Mills AM, et al. (2021). Elevated Neutrophil Gelatinase-Associated Lipocalin Is Associated With the Severity of Kidney Injury and Poor Prognosis of Patients With COVID-19. Kidney Int Rep 6, 2979–2992. 10.1016/j.ekir.2021.09.005. [PubMed: 34642645]
44. Staehli F, Ludigs K, Heinz LX, Seguin-Estevez Q, Ferrero I, Braun M, Schroder K, Rebsamen M, Tardivel A, Mattmann C, et al. (2012). NLRC5 deficiency selectively impairs MHC class I- dependent lymphocyte killing by cytotoxic T cells. J Immunol 188, 3820–3828. 10.4049/jimmunol.1102671. [PubMed: 22412192]
45. Zaki MH, Boyd KL, Vogel P, Kastan MB, Lamkanfi M, and Kanneganti TD (2010). The NLRP3 inflammasome protects against loss of epithelial integrity and mortality during experimental colitis. Immunity 32, 379–391. 10.1016/j.immuni.2010.03.003. [PubMed: 20303296]
46. Karki R, Sharma BR, Lee E, Banoth B, Malireddi RKS, Samir P, Tuladhar S, Mummareddy H, Burton AR, Vogel P, and Kanneganti TD (2020). Interferon regulatory factor 1 regulates PANoptosis to prevent colorectal cancer. JCI insight 5. 10.1172/jci.insight.136720.
47. Allen IC, TeKippe EM, Woodford RM, Uronis JM, Holl EK, Rogers AB, Herfarth HH, Jobin C, and Ting JP (2010). The NLRP3 inflammasome functions as a negative regulator of tumorigenesis during colitis-associated cancer. J Exp Med 207, 1045–1056. 10.1084/jem.20100050. [PubMed: 20385749]
48. Borges HL, Bird J, Wasson K, Cardiff RD, Varki N, Eckmann L, and Wang JY (2005). Tumor promotion by caspase-resistant retinoblastoma protein. Proc Natl Acad Sci U S A 102, 15587–15592. 10.1073/pnas.0503925102. [PubMed: 16227443]
49. Wang A, Pope SD, Weinstein JS, Yu S, Zhang C, Booth CJ, and Medzhitov R (2019). Specific sequences of infectious challenge lead to secondary hemophagocytic lymphohistiocytosis-like disease in mice. Proc Natl Acad Sci U S A 116, 2200–2209. 10.1073/pnas.1820704116. [PubMed: 30674681]
50. Karki R, Sharma BR, Tuladhar S, Williams EP, Zalduondo L, Samir P, Zheng M, Sundaram B, Banoth B, Malireddi RKS, et al. (2021). Synergism of TNF-alpha and IFN-gamma Triggers Inflammatory Cell Death, Tissue Damage, and Mortality in SARS-CoV-2 Infection and Cytokine Shock Syndromes. Cell 184, 149–168 e117. 10.1016/j.cell.2020.11.025. [PubMed: 33278357]
51. Chou WC, Jha S, Linhoff MW, and Ting JP (2023). The NLR gene family: from discovery to present day. Nat Rev Immunol 23, 635–654. 10.1038/s41577-023-00849-x. [PubMed: 36973360]
52. Sundaram B, Tweedell RE, Prasanth Kumar S, and Kanneganti TD (2024). The NLR family of innate immune and cell death sensors. Immunity 57, 674–699. 10.1016/j.immuni.2024.03.012. [PubMed: 38599165]
53. Kuriakose T, Man SM, Malireddi RK, Karki R, Kesavardhana S, Place DE, Neale G, Vogel P, and Kanneganti TD (2016). ZBP1/DAI is an innate sensor of influenza virus triggering the NLRP3 inflammasome and programmed cell death pathways. Sci Immunol 1. 10.1126/sciimmunol.aag2045.

54. Christgen S, and Kanneganti TD (2020). Inflammasomes and the fine line between defense and disease. Current Opin Immunol 62, 39–44. 10.1016/j.coi.2019.11.007.
55. Benko S, Magalhaes JG, Philpott DJ, and Girardin SE (2010). NLRC5 limits the activation of inflammatory pathways. J Immunol 185, 1681–1691. 10.4049/jimmunol.0903900. [PubMed: 20610642]
56. Kumar H, Pandey S, Zou J, Kumagai Y, Takahashi K, Akira S, and Kawai T (2011). NLRC5 deficiency does not influence cytokine induction by virus and bacteria infections. J Immunol 186, 994–1000. 10.4049/jimmunol.1002094. [PubMed: 21148033]
57. Knackstedt SL, Georgiadou A, Apel F, Abu-Abed U, Moxon CA, Cunnington AJ, Raupach B, Cunningham D, Langhorne J, Kruger R, et al. (2019). Neutrophil extracellular traps drive inflammatory pathogenesis in malaria. Sci Immunol 4. 10.1126/sciimmunol.aaw0336.
58. Filmann N, Rey J, Schneeweiss S, Ardizzone S, Bager P, Bergamaschi G, Koutroubakis I, Lindgren S, Morena Fde L, Moum B, et al. (2014). Prevalence of anemia in inflammatory bowel diseases in European countries: a systematic review and individual patient data meta-analysis. Inflamm Bowel Dis 20, 936–945. 10.1097/01.MIB.0000442728.74340.fd. [PubMed: 24572205]
59. Atug O, Kani HT, Banzragch M, Imeryuz N, and Akin H (2016). Incidence rate of anemia in inflammatory bowel diseases. Turk J Gastroenterol 27, 143–148. 10.5152/tjg.2016.16011. [PubMed: 27015619]
60. Gomollon F, and Gisbert JP (2009). Anemia and inflammatory bowel diseases. World J Gastroenterol 15, 4659–4665. 10.3748/wjg.15.4659. [PubMed: 19787829]
61. Kulnigg S, and Gasche C (2006). Systematic review: managing anaemia in Crohn's disease. Aliment Pharmacol Ther 24, 1507–1523. 10.1111/j.1365-2036.2006.03146.x. [PubMed: 17206940]
62. Holtzclaw JD, Jack D, Aguayo SM, Eckman JR, Roman J, and Hsu LL (2004). Enhanced pulmonary and systemic response to endotoxin in transgenic sickle mice. Am J Respir Crit Care Med 169, 687–695. 10.1164/rccm.200302-224OC. [PubMed: 14684557]
63. Botelho J, Machado V, Hussain SB, Zehra SA, Proenca L, Orlandi M, Mendes JJ, and D'Aiuto F (2021). Periodontitis and circulating blood cell profiles: a systematic review and meta-analysis. Exp Hematol 93, 1–13. 10.1016/j.exphem.2020.10.001. [PubMed: 33068648]
64. Michels K, Solomon AL, Scindia Y, Sordo Vieira L, Goddard Y, Whitten S, Vaulont S, Burdick MD, Atkinson C, Laubenbacher R, and Mehrad B (2022). Aspergillus Utilizes Extracellular Heme as an Iron Source During Invasive Pneumonia, Driving Infection Severity. J Infect Dis 225, 1811–1821. 10.1093/infdis/jiac079. [PubMed: 35267014]
65. Biffen RH (1905). Mendel's Laws of Inheritance and Wheat Breeding. J Ag Sci 1, 4–48. 10.1017/S0021859600000137.
66. van der Hoorn RA, and Kamoun S (2008). From Guard to Decoy: a new model for perception of plant pathogen effectors. Plant Cell 20, 2009–2017. 10.1105/tpc.108.060194. [PubMed: 18723576]
67. Jones JD, Vance RE, and Dangl JL (2016). Intracellular innate immune surveillance devices in plants and animals. Science 354. 10.1126/science.aaf6395.
68. Contreras MP, Lüdke D, Pai H, Toghani A, and Kamoun S (2023). NLR receptors in plant immunity: making sense of the alphabet soup. EMBO Rep 24, e57495. 10.15252/embr.202357495. [PubMed: 37602936]
69. HH F (1971). Current status of the gene-for-gene concept. Annu Rev Phytopathol 9, 275–296.
70. Shimizu M, Hirabuchi A, Sugihara Y, Abe A, Takeda T, Kobayashi M, Hiraka Y, Kanzaki E, Oikawa K, Saitoh H, et al. (2022). A genetically linked pair of NLR immune receptors shows contrasting patterns of evolution. Proc Natl Acad Sci U S A 119, e2116896119. 10.1073/pnas.2116896119. [PubMed: 35771942]
71. Yang J, Zhao Y, Shi J, and Shao F (2013). Human NAIP and mouse NAIP1 recognize bacterial type III secretion needle protein for inflammasome activation. Proc Natl Acad Sci U S A 110, 14408–14413. 10.1073/pnas.1306376110. [PubMed: 23940371]
72. Reyes Ruiz VM, Ramirez J, Naseer N, Palacio NM, Siddarthan IJ, Yan BM, Boyer MA, Pensinger DA, Sauer JD, and Shin S (2017). Broad detection of bacterial type III secretion system and

flagellin proteins by the human NAIP/NLRC4 inflammasome. Proc Natl Acad Sci U S A 114, 13242–13247. 10.1073/pnas.1710433114. [PubMed: 29180436]

73. Grandjean T, Boucher A, Thepaut M, Monlezun L, Guery B, Faudry E, Kipnis E, and Dessein R (2017). The human NAIP-NLRC4-inflammasome senses the Pseudomonas aeruginosa T3SS inner-rod protein. Int Immunol 29, 377–384. 10.1093/intimm/dxx047. [PubMed: 28992059]
74. Zhao Y, Yang J, Shi J, Gong YN, Lu Q, Xu H, Liu L, and Shao F (2011). The NLRC4 inflammasome receptors for bacterial flagellin and type III secretion apparatus. Nature 477, 596–600. 10.1038/nature10510. [PubMed: 21918512]
75. Kofoed EM, and Vance RE (2011). Innate immune recognition of bacterial ligands by NAIPs determines inflammasome specificity. Nature 477, 592–595. 10.1038/nature10394. [PubMed: 21874021]
76. Zaki MH, Vogel P, Malireddi RK, Body-Malapel M, Anand PK, Bertin J, Green DR, Lamkanfi M, and Kanneganti TD (2011). The NOD-like receptor NLRP12 attenuates colon inflammation and tumorigenesis. Cancer Cell 20, 649–660. 10.1016/j.ccr.2011.10.022. [PubMed: 22094258]
77. Allen IC, Wilson JE, Schneider M, Lich JD, Roberts RA, Arthur JC, Woodford RM, Davis BK, Uronis JM, Herfarth HH, et al. (2012). NLRP12 suppresses colon inflammation and tumorigenesis through the negative regulation of noncanonical NF-kappaB signaling. Immunity 36, 742–754. 10.1016/j.immuni.2012.03.012. [PubMed: 22503542]
78. Chen GY (2014). Role of Nlrp6 and Nlrp12 in the maintenance of intestinal homeostasis. Eur J Immunol 44, 321–327. 10.1002/eji.201344135. [PubMed: 24338634]
79. Chen L, Wilson JE, Koenigsknecht MJ, Chou WC, Montgomery SA, Truax AD, Brickey WJ, Packey CD, Maharshak N, Matsushima GK, et al. (2017). NLRP12 attenuates colon inflammation by maintaining colonic microbial diversity and promoting protective commensal bacterial growth. Nat Immunol 18, 541–551. 10.1038/ni.3690. [PubMed: 28288099]
80. Khan S, Kwak YT, Peng L, Hu S, Cantarel BL, Lewis CM, Gao Y, Mani RS, Kanneganti TD, and Zaki H (2023). NLRP12 downregulates the Wnt/beta-catenin pathway via interaction with STK38 to suppress colorectal cancer. J Clin Invest 133. 10.1172/JCI166295.
81. Coombs JR, Zamoshnikova A, Holley CL, Maddugoda MP, Teo DET, Chauvin C, Poulin LF, Vitak N, Ross CM, Mellacheruvu M, et al. (2024). NLRP12 interacts with NLRP3 to block the activation of the human NLRP3 inflammasome. Sci Signal 17, eabg8145. 10.1126/scisignal.abg8145. [PubMed: 38261657]
82. Vladimer GI, Weng D, Paquette SW, Vanaja SK, Rathinam VA, Aune MH, Conlon JE, Burbage JJ, Proulx MK, Liu Q, et al. (2012). The NLRP12 inflammasome recognizes Yersinia pestis. Immunity 37, 96–107. 10.1016/j.immuni.2012.07.006. [PubMed: 22840842]
83. Ataide MA, Andrade WA, Zamboni DS, Wang D, Souza Mdo C, Franklin BS, Elian S, Martins FS, Pereira D, Reed G, et al. (2014). Malaria-induced NLRP12/NLRP3-dependent caspase-1 activation mediates inflammation and hypersensitivity to bacterial superinfection. PLoS Pathog 10, e1003885. 10.1371/journal.ppat.1003885. [PubMed: 24453977]
84. Man SM, Karki R, Malireddi RK, Neale G, Vogel P, Yamamoto M, Lamkanfi M, and Kanneganti TD (2015). The transcription factor IRF1 and guanylate-binding proteins target activation of the AIM2 inflammasome by Francisella infection. Nat Immunol 16, 467–475. 10.1038/ni.3118. [PubMed: 25774715]
85. Hoffmann E, Neumann G, Kawaoka Y, Hobom G, and Webster RG (2000). A DNA transfection system for generation of influenza A virus from eight plasmids. Proc Natl Acad Sci U S A 97, 6108–6113. 10.1073/pnas.100133697. [PubMed: 10801978]
86. Kanneganti TD, Ozoren N, Body-Malapel M, Amer A, Park JH, Franchi L, Whitfield J, Barchet W, Colonna M, Vandenabeele P, et al. (2006). Bacterial RNA and small antiviral compounds activate caspase-1 through cryopyrin/Nalp3. Nature 440, 233–236. 10.1038/nature04517. [PubMed: 16407888]
87. Takeuchi O, Hoshino K, Kawai T, Sanjo H, Takada H, Ogawa T, Takeda K, and Akira S (1999). Differential roles of TLR2 and TLR4 in recognition of gram-negative and gram-positive bacterial cell wall components. Immunity 11, 443–451. 10.1016/s1074-7613(00)80119-3. [PubMed: 10549626]

88. Hoshino K, Takeuchi O, Kawai T, Sanjo H, Ogawa T, Takeda Y, Takeda K, and Akira S (1999). Cutting edge: Toll-like receptor 4 (TLR4)-deficient mice are hyporesponsive to lipopolysaccharide: evidence for TLR4 as the Lps gene product. J Immunol 162, 3749–3752. [PubMed: 10201887]

89. Ishii KJ, Kawagoe T, Koyama S, Matsui K, Kumar H, Kawai T, Uematsu S, Takeuchi O, Takeshita F, Coban C, and Akira S (2008). TANK-binding kinase-1 delineates innate and adaptive immune responses to DNA vaccines. Nature 451, 725–729. 10.1038/nature06537. [PubMed: 18256672]

90. Mariathasan S, Newton K, Monack DM, Vucic D, French DM, Lee WP, Roose-Girma M, Erickson S, and Dixit VM (2004). Differential activation of the inflammasome by caspase-1 adaptors ASC and Ipaf. Nature 430, 213–218. 10.1038/nature02664. [PubMed: 15190255]

91. Kayagaki N, Warming S, Lamkanfi M, Vande Walle L, Louie S, Dong J, Newton K, Qu Y, Liu J, Heldens S, et al. (2011). Non-canonical inflammasome activation targets caspase-11. Nature 479, 117–121. 10.1038/nature10558. [PubMed: 22002608]

92. Jones JW, Kayagaki N, Broz P, Henry T, Newton K, O'Rourke K, Chan S, Dong J, Qu Y, Roose-Girma M, et al. (2010). Absent in melanoma 2 is required for innate immune recognition of Francisella tularensis. Proc Natl Acad Sci U S A 107, 9771–9776. 10.1073/pnas.1003738107. [PubMed: 20457908]

93. Gurung P, Burton A, and Kanneganti TD (2016). NLRP3 inflammasome plays a redundant role with caspase 8 to promote IL-1beta-mediated osteomyelitis. Proc Natl Acad Sci U S A 113, 4452–4457. 10.1073/pnas.1601636113. [PubMed: 27071119]

94. Oberst A, Dillon CP, Weinlich R, McCormick LL, Fitzgerald P, Pop C, Hakem R, Salvesen GS, and Green DR (2011). Catalytic activity of the caspase-8-FLIP(L) complex inhibits RIPK3-dependent necrosis. Nature 471, 363–367. 10.1038/nature09852. [PubMed: 21368763]

95. Pelletier S, Gingras S, and Green DR (2015). Mouse genome engineering via CRISPR-Cas9 for study of immune function. Immunity 42, 18–27. 10.1016/j.immuni.2015.01.004. [PubMed: 25607456]

96. Bae S, Park J, and Kim JS (2014). Cas-OFFinder: a fast and versatile algorithm that searches for potential off-target sites of Cas9 RNA-guided endonucleases. Bioinformatics 30, 1473–1475. 10.1093/bioinformatics/btu048. [PubMed: 24463181]

97. Rossi M, Delbauve S, Wespes E, Roumeguere T, Leo O, Flamand V, Le Moine A, and Hougardy JM (2018). Dual effect of hemin on renal ischemia-reperfusion injury. Biochem Biophys Res Commun 503, 2820–2825. 10.1016/j.bbrc.2018.08.046. [PubMed: 30100067]

98. Zheng M, Karki R, Vogel P, and Kanneganti TD (2020). Caspase-6 Is a Key Regulator of Innate Immunity, Inflammasome Activation, and Host Defense. Cell 181, 674–687 e613. 10.1016/j.cell.2020.03.040. [PubMed: 32298652]

99. Love MI, Huber W, and Anders S (2014). Moderated estimation of fold change and dispersion for RNA-seq data with DESeq2. Genome Biol. 15, 550. 10.1186/s13059-014-0550-8. [PubMed: 25516281]

100. Benjamini Y, and Hochberg Y (1995). Controlling the false discovery rate: a practical and powerful approach to multiple testing. J. R. Stat. Soc. Series B Stat. Methodol. 57, 289–300.

101. Gu Z, Eils R, and Schlesner M (2016). Complex heatmaps reveal patterns and correlations in multidimensional genomic data. Bioinformatics 32, 2847–2849. 10.1093/bioinformatics/btw313. [PubMed: 27207943]

102. Christgen S, Zheng M, Kesavardhana S, Karki R, Malireddi RKS, Banoth B, Place DE, Briard B, Sharma BR, Tuladhar S, et al. (2020). Identification of the PANoptosome: A Molecular Platform Triggering Pyroptosis, Apoptosis, and Necroptosis (PANoptosis). Front Cell Infect Microbiol 10, 237. 10.3389/fcimb.2020.00237. [PubMed: 32547960]

Highlights

- NLRC5 functions as an innate immune sensor in hemolytic and inflammatory conditions
- NLRC5 regulates PANoptosome formation and innate immune cell death, PANoptosis
- TLRs and NAD^+ regulate NLRC5 expression and ROS production to induce PANoptosis
- Deletion of NLRC5 protects mice from colitis, HLH, and hemolytic disease

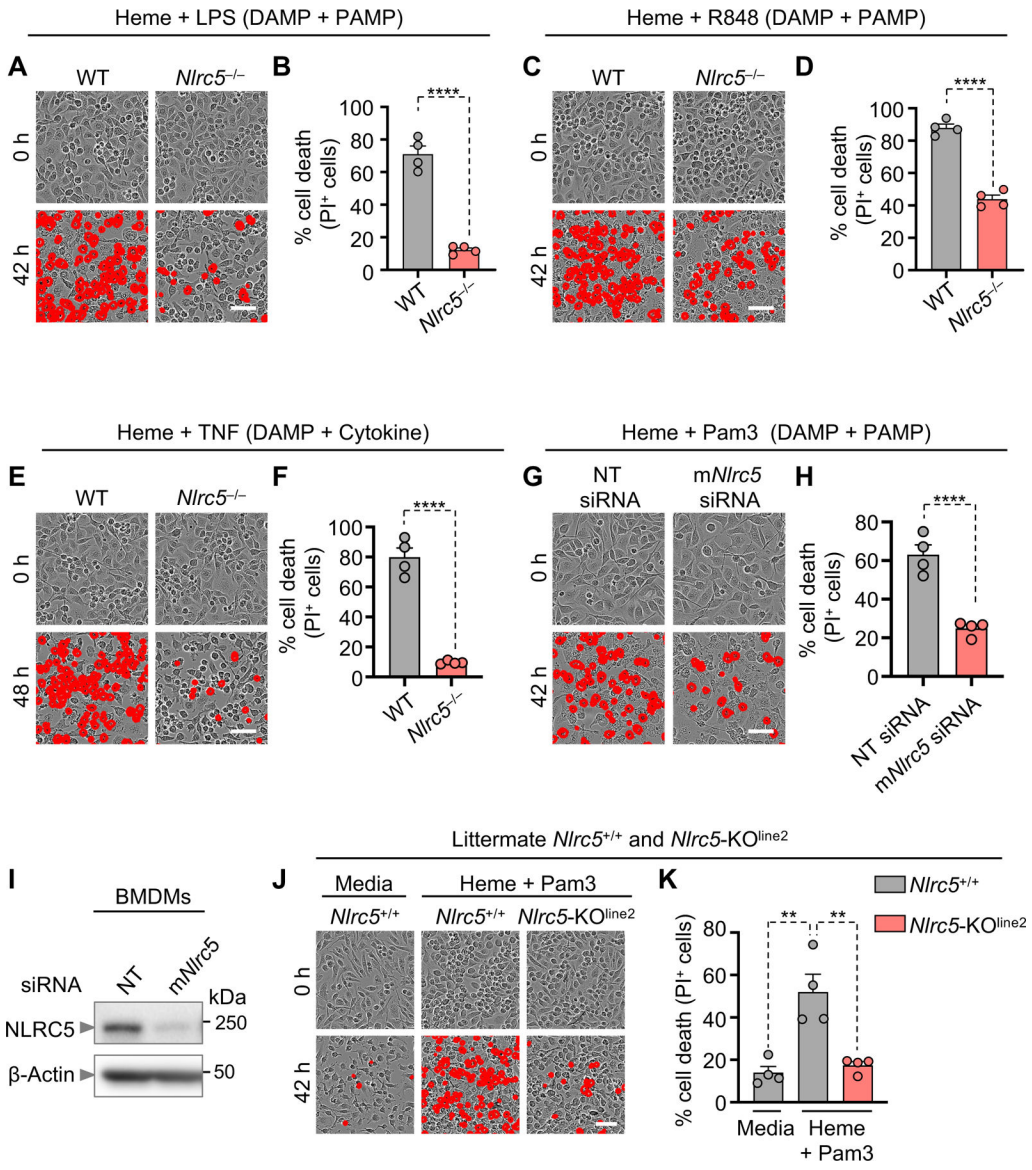

Figure 1. NLRC5 mediates inflammatory cell death in response to heme plus PAMP or heme plus cytokine triggers

(A and B) Cell death images (A) and quantification of cell death (B) using wild-type (WT) and *Nlrc5*$^{-/-}$ bone marrow-derived macrophages (BMDMs) in response to heme plus lipopolysaccharide (LPS) treatment for 42 h. (C and D) Cell death images (C) and quantification of cell death (D) using WT and *Nlrc5*$^{-/-}$ BMDMs stimulated with heme plus Resiquimod (R848) for 42 h. (E and F) Cell death images (E) and quantification of cell death (F) using WT and *Nlrc5*$^{-/-}$ BMDMs treated with heme plus TNF for 48 h. (G and H) Cell death images (G) and quantification of cell death (H) using BMDMs electroporated with control (non-targeting, NT) siRNA or mouse *Nlrc5*-targeting siRNA, then treated with heme and Pam3CSK4 (Pam3) for 42 h. (I) Western blot analysis of NLRC5 expression in BMDMs electroporated with control or mouse *Nlrc5*-targeting siRNA. For loading control, β-actin is shown. (J and K) Cell death images (J) and quantification of cell death (K) in littermate *Nlrc5*$^{+/+}$ and *Nlrc5*-KO^{line2} BMDMs treated with heme plus Pam3 for 42 h. Scale

bar = 50 μm (A, C, E, G, and J). *Nlrc5*$^{-/-}$ BMDMs (ref. [56]) (A–F) and *Nlrc5*-KO^{line2} BMDMs (J and K) were used for stimulation. Three or more independent experiments were performed, and the data shown are from a single experiment that is representative. Mean ± SEM are shown (B, D, F, H, and K). Statistical analyses were performed using the unpaired t test (B, D, F, and H) or the one-way ANOVA (K). $^{**}P < 0.01$; $^{****}P < 0.0001$.
See also Figures S1, S2, and S3.

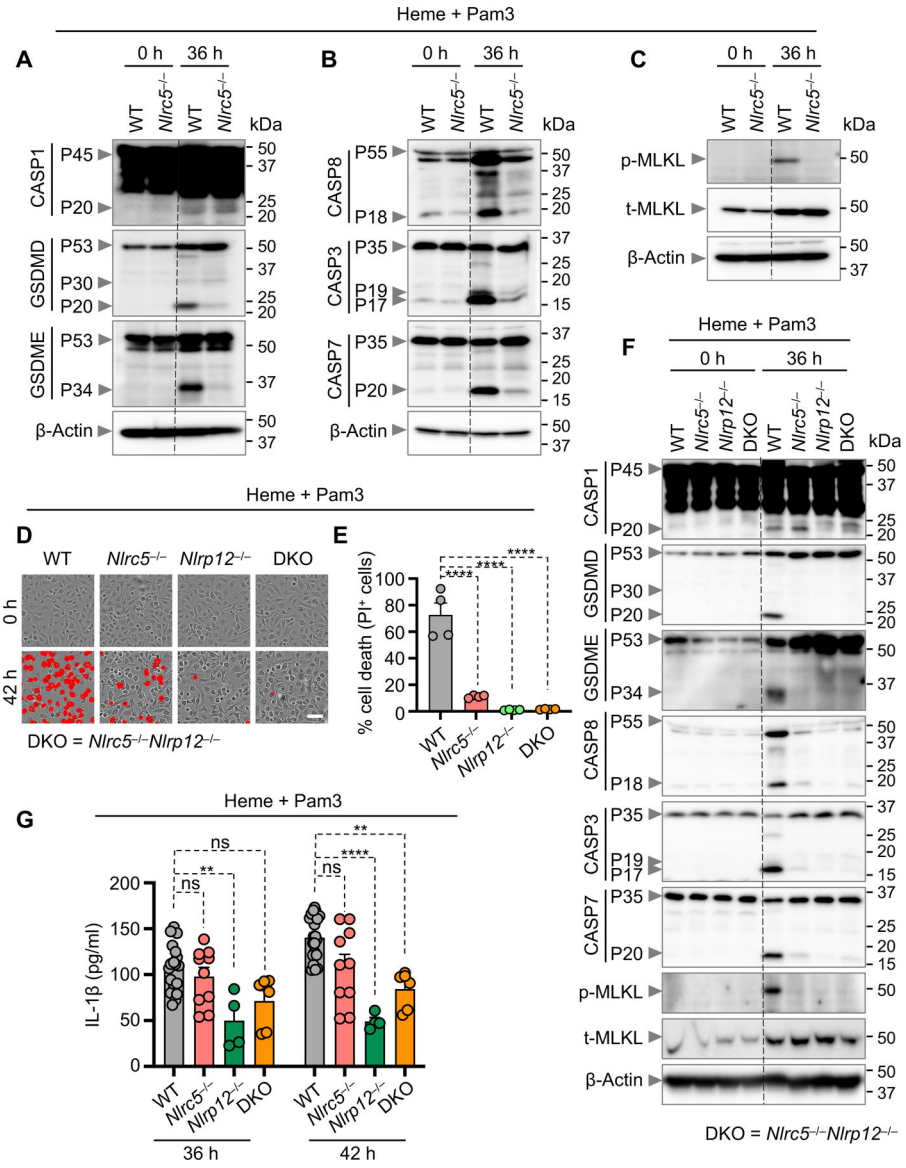

Figure 2. NLRC5 regulates inflammatory cell death in response to heme plus PAMPs

(A–C) Western blot analysis of (A) pro- and activated caspase-1 (CASP1; P45 and P20, respectively); pro-, activated, and inactivated gasdermin D (GSDMD; P53, P30, and P20, respectively); and pro- and activated gasdermin E (GSDME; P53 and P34, respectively); (B) pro- and cleaved caspase-8 (CASP8; P55 and P18, respectively); pro- and cleaved caspase-3 (CASP3; P35 and P19/P17, respectively); pro- and cleaved caspase-7 (CASP7; P35 and P20, respectively); and (C) phosphorylated and total MLKL (p-MLKL and t-MLKL) in wild-type (WT) and *Nlrc5*$^{-/-}$ bone marrow-derived macrophages (BMDMs) at 0 h or following treatment with heme plus Pam3CSK4 (Pam3) for 36 h. For loading control, β-actin is shown. (D and E) Cell death images (D) and quantification of cell death (E) using WT, *Nlrc5*$^{-/-}$, *Nlrp12*$^{-/-}$, and *Nlrc5*$^{-/-}$*Nlrp12*$^{-/-}$ (DKO) BMDMs in response to heme plus Pam3 treatment for 42 h. (F) Western blot analysis of CASP1, GSDMD, GSDME, CASP8, CASP3, CASP7, p-MLKL, and t-MLKL in WT, *Nlrc5*$^{-/-}$, *Nlrp12*$^{-/-}$, and DKO

BMDMs at 0 h or following treatment with heme plus Pam3 for 36 h. For loading control, β-actin is shown. (G) Measurement of IL-1β release in the supernatant of WT, *Nlrc5*$^{-/-}$, *Nlrp12*$^{-/-}$, and DKO BMDMs following treatment with heme plus Pam3 for 36 h or 42 h. Scale bar = 50 μm (D). *Nlrc5*$^{-/-}$ BMDMs (ref. [56]) (A–G) were used for stimulation. Three or more independent experiments were performed, and the data shown are from a single experiment that is representative. Mean ± SEM are shown (E and G). Statistical analyses were performed using the one-way ANOVA (E) or the two-way ANOVA (G). ns, not significant; ** $P < 0.01$; **** $P < 0.0001$.

See also Figure S4.

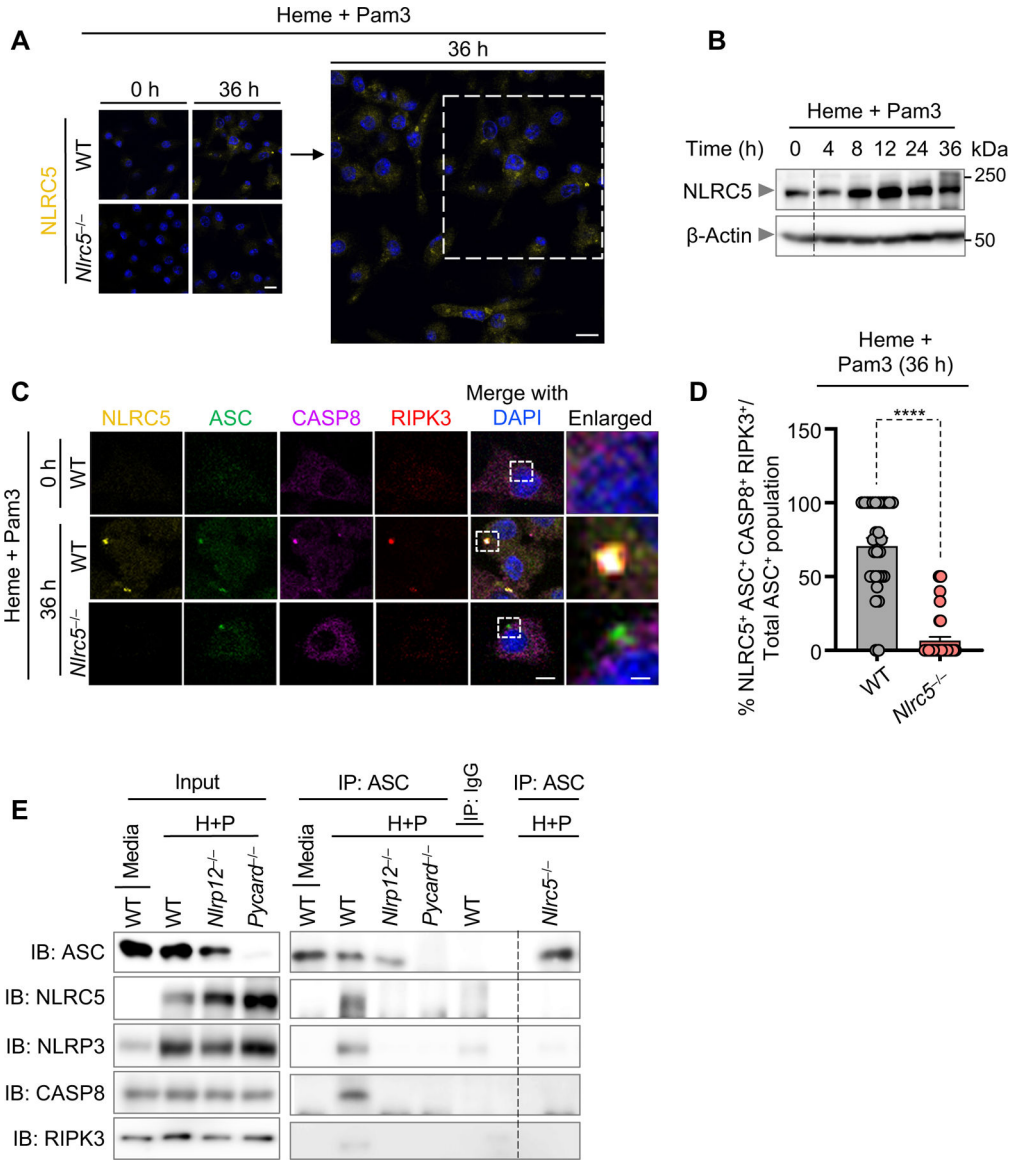

Figure 3. NLRC5 interacts with NLRP12 to form a multiprotein cell death-inducing complex

(A) Wild-type (WT) and *Nlrc5*$^{-/-}$ bone marrow-derived macrophages (BMDMs) were either left unstimulated (0 h) or treated with heme plus Pam3CSK4 (Pam3) for 36 h and stained for NLRC5, and counter-stained with DAPI to visualize nuclei. A broader, enlarged field of view for WT BMDMs at the 36 h timepoint is shown. (B) Western blot analysis of NLRC5 in WT BMDMs stimulated with heme plus Pam3 for the indicated times. For loading control, β-actin is shown. (C) WT and *Nlrc5*$^{-/-}$ BMDMs were either unstimulated (0 h) or treated with heme plus Pam3 for 36 h and stained for NLRC5, ASC, caspase-8 (CASP8), and RIPK3, and counter-stained with DAPI to visualize nuclei. Representative images of cells containing co-localized NLRC5, ASC, CASP8, and RIPK3 are shown. The magnified view of the boxed area (merged) is shown on the right (enlarged). (D) Quantification showing the percentage of cells with NLRC5^{+}ASC^{+} CASP8^{+} RIPK3^{+} specks out of the total population of cells with ASC^{+} specks in WT and *Nlrc5*$^{-/-}$ BMDMs at 36

h post-stimulation with heme plus Pam3. Each data point indicates a single field of view (average n = 103 cells per field). (E) Immunoblot analysis (IB) of ASC, NLRC5, NLRP3, CASP8, and RIPK3 following immunoprecipitation (IP) with IgG control or anti-ASC antibodies in WT, *Nlrp12*$^{-/-}$, *Pycard*$^{-/-}$, and *Nlrc5*$^{-/-}$ BMDMs after treatment with heme plus Pam3 (H+P) for 28 h. Scale bars = 10 μm (A), 5 μm (C, merge column), and 1 μm (C, enlarged column). *Nlrc5*$^{-/-}$ BMDMs (ref. [56]) (A, C–E) were used for stimulation. Three or more independent experiments were performed, and the data shown are from a single experiment that is representative. Mean ± SEM are shown (D). Statistical analyses were performed using the unpaired t test (D). **** $P < 0.0001$.

See also Figure S5.

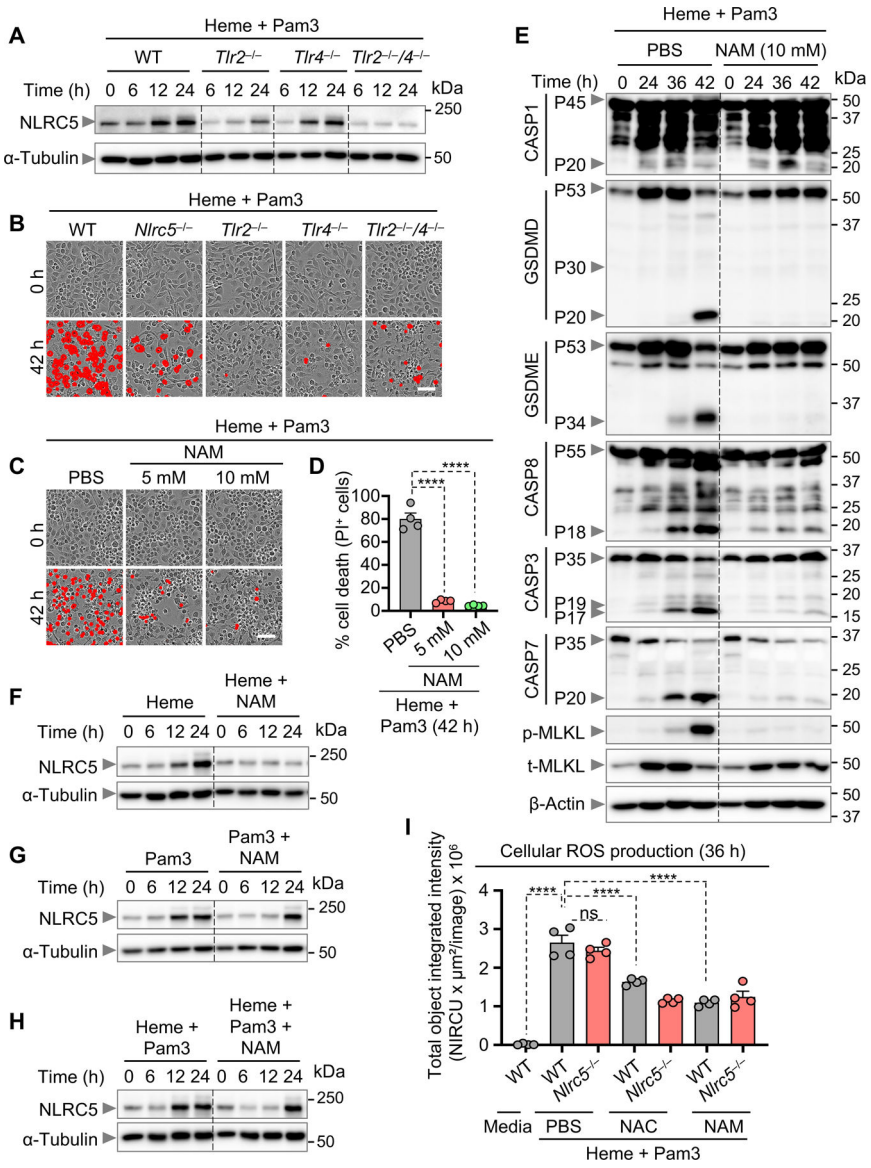

Figure 4. Membrane-bound TLR and NAD$^+$ signaling mediate NLRC5 expression and ROS production to modulate inflammatory cell death

(A) Western blot analysis of NLRC5 expression in wild-type (WT), *Tlr2*$^{-/-}$, *Tlr4*$^{-/-}$, and *Tlr2*$^{-/-}$/*Tlr4*$^{-/-}$ (*Tlr2*$^{-/-}$/*4*$^{-/-}$) bone marrow-derived macrophages (BMDMs) treated with heme plus Pam3CSK4 (Pam3) for the indicated times. (B) Images representing cell death occurrences in WT, *Nlrc5*$^{-/-}$, *Tlr2*$^{-/-}$, *Tlr4*$^{-/-}$, and *Tlr2*$^{-/-}$/*4*$^{-/-}$ BMDMs at 0 h or following treatment with heme plus Pam3 for 42 h. (C and D) Images representing cell death occurrences (C) and quantification of cell death (D) in WT BMDMs at 0 h or following treatment with heme plus Pam3 with and without nicotinamide (NAM) for 42 h. (E) Western blot analysis of pro- and activated caspase-1 (CASP1; P45 and P20, respectively); pro-, activated, and inactivated gasdermin D (GSDMD; P53, P30, and P20, respectively); pro- and activated gasdermin E (GSDME; P53 and P34, respectively); pro- and cleaved caspase-8 (CASP8; P55 and P18, respectively); pro- and cleaved caspase-3 (CASP3; P35 and P19/P17, respectively); pro- and cleaved caspase-7 (CASP7; P35 and P20,

respectively); phosphorylated and total MLKL (p-MLKL and t-MLKL) in WT BMDMs following treatment with heme plus Pam3 with and without NAM for the indicated times. For loading control, β-actin is shown. (F–H) Western blot analysis of NLRC5 in WT BMDMs stimulated with heme (F), Pam3 (G), or heme plus Pam3 (H) with and without NAM for the indicated times. For loading control, α-Tubulin is shown. (I) Quantification of total fluorescence intensity of cellular ROS in WT and *Nlrc5*$^{-/-}$ BMDMs in response to media alone or heme plus Pam3 treatment with and without NAC or NAM for 36 h. Scale bar = 50 μm (B and C). *Nlrc5*$^{-/-}$ BMDMs (ref. [56]) (B and I) were used for stimulation. Three or more independent experiments were performed, and the data shown are from a single experiment that is representative. Mean ± SEM are shown (D and I). Statistical analyses were performed using the one-way ANOVA (D and I). ns, not significant; **** $P < 0.0001$.

See also Figure S5.

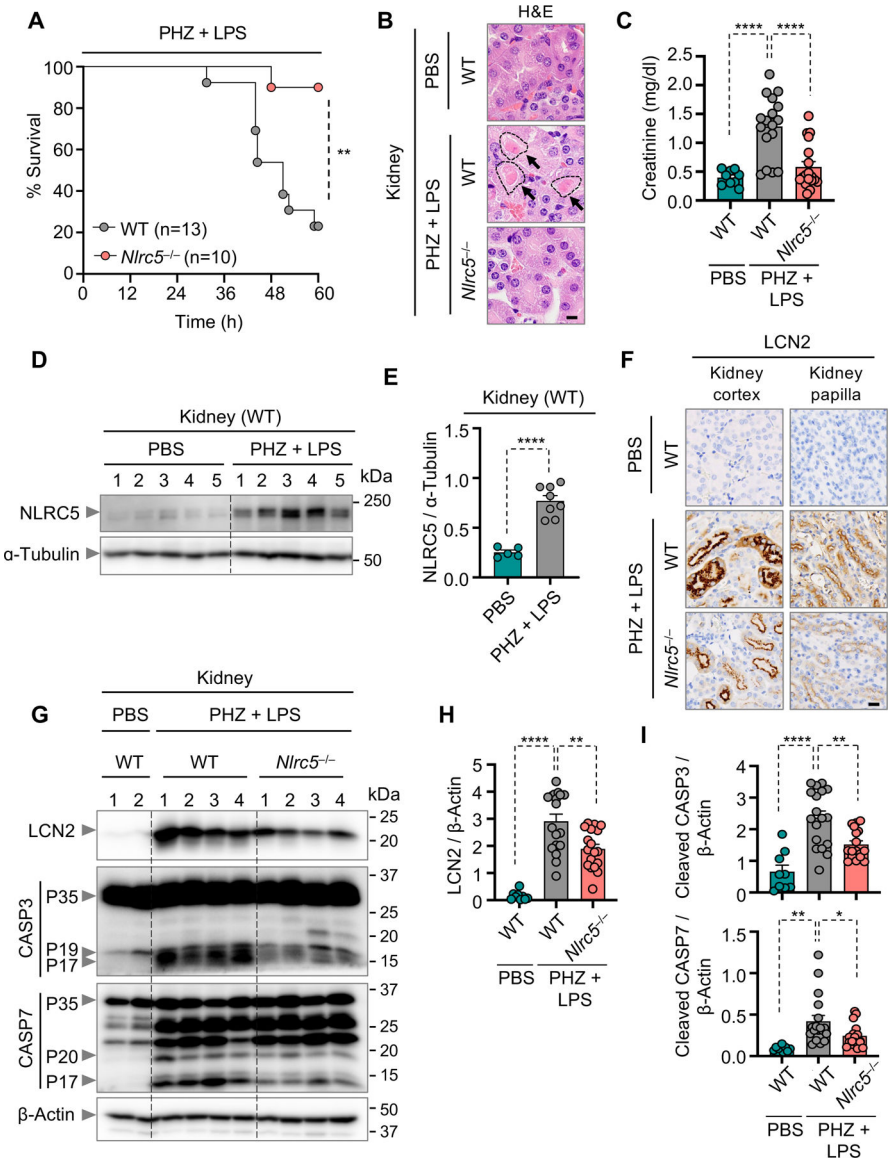

Figure 5. NLRC5 drives renal tissue damage and lethality in hemolytic disease model

(A) Survival of 8- to 10-week-old male wild-type (WT) (n = 13) and *Nlrc5*$^{-/-}$ (n = 10) mice after intraperitoneal injection of phenylhydrazine (PHZ) plus lipopolysaccharide (LPS). (B) Representative images showing hematoxylin and eosin (H&E)-stained kidney sections from WT and *Nlrc5*$^{-/-}$ mice 30 h after PBS or PHZ plus LPS injection. Outlined areas and arrows denote degenerating kidney tubular epithelium. Images are representative of n = 9 WT (PBS), n = 17 WT (PHZ + LPS), and n = 18 *Nlrc5*$^{-/-}$ (PHZ + LPS) mice. (C) Serum creatinine levels in WT and *Nlrc5*$^{-/-}$ mice injected with PBS (WT, n = 9) or PHZ plus LPS (WT, n = 17 and *Nlrc5*$^{-/-}$, n = 18) at 30 h post-treatment. (D) Western blot analysis of NLRC5 in kidney tissue from WT mice following treatment with PBS or PHZ plus LPS at 30 h post-treatment. For loading control, α-Tubulin is shown. (E) Densitometric quantification of NLRC5 expression normalized to α-Tubulin expression from WT mice injected with PBS or PHZ plus LPS at 30 h post-treatment (PBS, n = 5; PHZ + LPS, n =

8). (F) Representative images of lipocalin 2 (LCN2) staining in kidney cortex and papilla of WT and *Nlrc5*$^{-/-}$ mice 30 h after PBS or PHZ plus LPS injection. Images are representative of n = 9 WT (PBS), n = 17 WT (PHZ + LPS), and n = 18 *Nlrc5*$^{-/-}$ (PHZ + LPS) mice. (G) Western blot analysis of LCN2; pro- and cleaved caspase-3 (CASP3; P35 and P19/P17, respectively); and pro- and cleaved caspase-7 (CASP7; P35 and P20/P17, respectively) in kidney tissue from WT and *Nlrc5*$^{-/-}$ mice treated with PBS or PHZ plus LPS at 30 h post-treatment. For loading control, β-actin is shown. (H and I) Densitometric quantification of LCN2 (H) and cleaved CASP3 and cleaved CASP7 (I) expression normalized to β-actin expression from WT and *Nlrc5*$^{-/-}$ mice treated with PBS (WT = 9) or PHZ plus LPS (WT, n = 17 and *Nlrc5*$^{-/-}$, n = 18) at 30 h post-treatment. Scale bar = 20 μm (B and F). Mean ± SEM are shown (C, E, H, and I). *Nlrc5*$^{-/-}$ mice (ref. [56]) (A–C and F–I) were used for PHZ plus LPS injection. Two independent experiments were performed to assess survival, and two independent experiments were performed to assess serum parameters, histology, and cell death molecule activation. Pooled results are shown. Statistical analyses were performed using the log-rank (Mantel-Cox) test (A), the one-way ANOVA (C, H, and I), or the unpaired t test (E). *$P < 0.05$; **$P < 0.01$; ****$P < 0.0001$.
See also Figure S6.

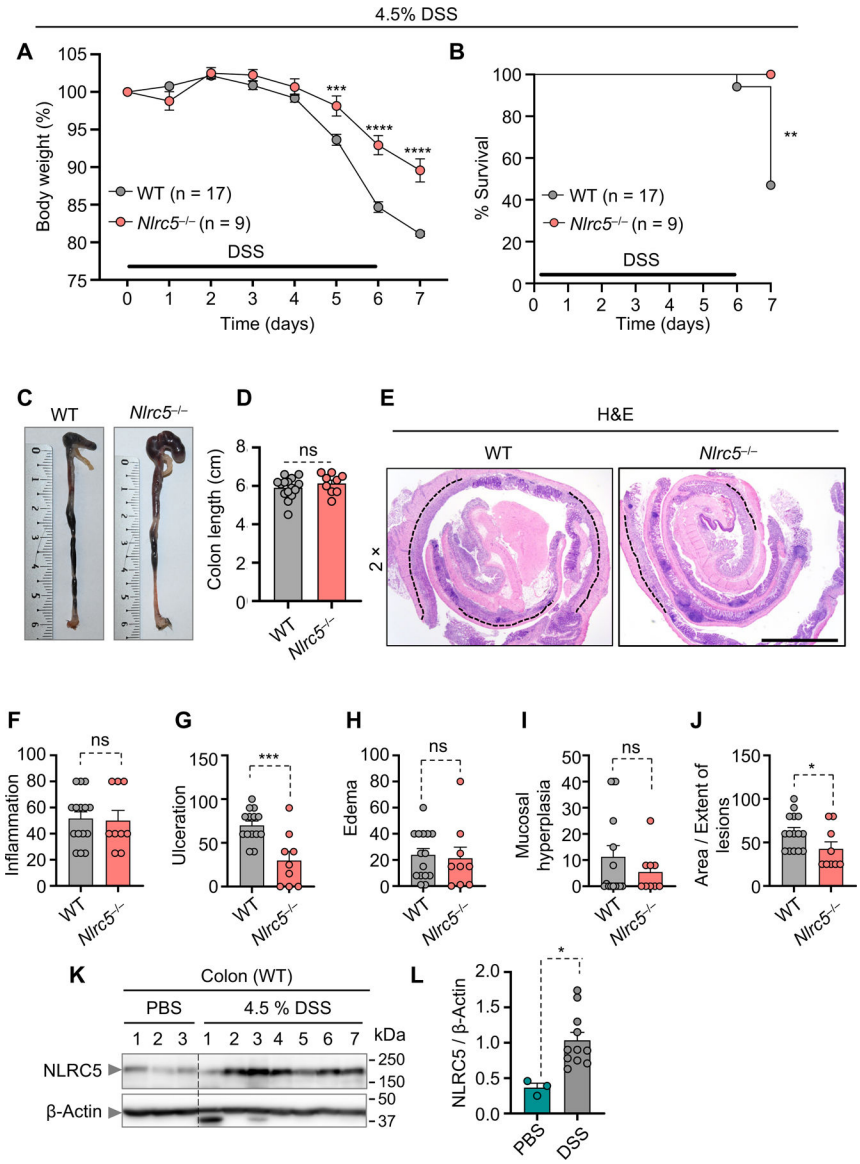

Figure 6. NLRC5 drives colon inflammation and pathogenesis in a colitis model

(A–B) Wild-type (WT) (n = 17) and *Nlrc5*$^{-/-}$ (n = 9) mice were treated with 4.5% dextran sodium sulfate (DSS) in drinking water for 6 days. Body weight (A) and survival (B) were monitored until day 7. (C and D) Images showing representative colon length (C) and measurements of colon length (D) from WT (n = 15) and *Nlrc5*$^{-/-}$ (n = 9) mice on day 7 after DSS administration. (E) Representative images showing hematoxylin and eosin (H&E)-stained colon sections from WT and *Nlrc5*$^{-/-}$ mice on day 7 after DSS administration. Dotted lines denote the ulcerated areas. Images are representative of n = 15 WT and n = 9 *Nlrc5*$^{-/-}$ mice. (F–J) Quantification of histological scores for inflammation (F), ulceration (G), edema (H), mucosal hyperplasia (I), and extent of lesions (J) from WT and *Nlrc5*$^{-/-}$ mice on day 7 after DSS administration. (K) Western blot analysis of NLRC5 in kidney tissues from WT mice on day 7 after PBS or DSS treatment. For loading control, β-actin is shown. (L) Densitometric quantification of NLRC5 expression normalized to β-

actin expression from WT mice on day 7 after PBS (n = 3) or DSS treatment (n = 11 mice). Mean ± SEM are shown (A, D, F–J, and L). Scale bar = 2 mm (E). *Nlrc5*$^{-/-}$ mice (ref. [56]) (A–J) were used for DSS treatment. Two independent experiments were performed to assess body weight, survival, and histology. Pooled results are shown. Statistical analyses were performed using the two-way ANOVA (A), log-rank (Mantel-Cox) test (B), or unpaired t test (D, F–J, and L). ns, not significant; *$P < 0.05$; **$P < 0.01$; ***$P < 0.001$; ****$P < 0.0001$.

See also Figure S6.

Key Resources Table

REAGENT or RESOURCE	SOURCE	IDENTIFIER
Antibodies		
anti-caspase-3	Cell Signaling Technology	Cat# 9662; RRID:AB_331439
anti-cleaved caspase-3	Cell Signaling Technology	Cat# 9661; RRID:AB_2341188
anti-caspase-7	Cell Signaling Technology	Cat# 9492; RRID:AB_2228313
anti-cleaved caspase-7	Cell Signaling Technology	Cat# 9491; RRID:AB_2068144
anti-caspase-8	Cell Signaling Technology	Cat# 4927; RRID: AB_2068301
anti-cleaved caspase-8	Cell Signaling Technology	Cat# 8592; RRID:AB_10891784
anti-pMLKL	Cell Signaling Technology	Cat# 37333; RRID:AB_2799112
anti-tMLKL	Abgent	Cat# AP14272b; RRID:AB_11134649
anti-GSDMD	Abcam	Cat# ab209845; RRID:AB_2783550
anti-GSDME	Abcam	Cat# ab215191; RRID:AB_2737000
anti-caspase-1	AdipoGen	Cat# AG-20B-0044; RRID:AB_2490253
anti-NLRC5 [clone E1E9Y]	Cell Signaling Technology (This paper)	Cat# 72379
anti-Lipocalin 2 [EPR21092] (for WB)	Abcam	Cat# ab216462
anti-Lipocalin 2 (for IHC)	Novus Biologicals	Cat# NBP1-05183; RRID:AB_1556264
anti-mouse CD8 (for IHC)	eBioscience	Cat# 14-0808-82 RRID: AB_2572861
anti-α-Tubulin	Cell Signaling Technology	Cat# 2144; RRID: AB_2210548
anti-ASC (for IF)	Millipore	Cat# 04-147; RRID:AB_1977033
Anti-RIPK3 (for IF)	Millipore	Cat# MABC1595; RRID: AB_2940810
Isotype control IgG antibody	Cell Signaling Technology	Cat# 3900S; RRID:AB_1550038
anti-ASC (for IP and WB)	AdipoGen	Cat# AG-25B-0006; RRID:AB_2885200
anti-caspase-8 (for IP, WB, and IF)	AdipoGen	Cat# AG-20T-0138-C100 RRID: AB_2490519
anti-RIPK3 (for WB)	Prosci	Cat# 2283; RRID: AB_203256
anti-human NLRP12 (for IP)	Abcepta	Cat# AP14014a; RRID:AB_10893749
anti-RIPK3 (for IP)	Santa Cruz	Cat# sc-374639; RRID:AB_10332232
anti-Myc	Cell Signaling Technology	Cat# 2276; RRID:AB_331783
anti-NLRP3	AdipoGen	Cat# AG-20B-0014 RRID: AB_2490202
anti-FLAG	Sigma	Cat# F1804; RRID: AB_262044
anti-HA	Cell Signaling Technology	Cat# 2367; RRID:AB_10691311
anti-human caspase-8	Enzo Life Science	Cat# ALX-804-242; RRID:AB_2259459
HRP-conjugated anti-GAPDH	Santa Cruz Biotechnology	Cat# sc-166574; RRID:AB_2107296
HRP-conjugated anti-β-actin	Santa Cruz Biotechnology	Cat# sc-47778; RRID:AB_2714189
HRP-conjugated secondary anti-rabbit	Jackson ImmunoResearch Laboratories	Cat# 111-035-047; RRID:AB_2337940
HRP-conjugated secondary anti-mouse	Jackson ImmunoResearch Laboratories	Cat# 315-035-047; RRID:AB_2340068
HRP-conjugated secondary anti-rat	Jackson ImmunoResearch Laboratories	Cat# 112-035-143; RRID:AB_2338138

REAGENT or RESOURCE	SOURCE	IDENTIFIER
anti-mouse IgG AlexaPlus-488	Thermo Fisher Scientific	Cat# A32723; RRID: AB_2633275
goat anti-rat IgG Alexa-568	Thermo Fisher Scientific	Cat# A11077; RRID: AB_2534121
goat anti-rabbit IgG Alexaflour-633	Thermo Fisher Scientific	Cat# A-21070 RRID: AB_2535731
goat anti-rabbit IgG AlexaPlus-647	Thermo Fisher Scientific	Cat# A32733; RRID: AB_2633282
rat IgG isotype control (For IF)	Thermo Fisher Scientific	Cat# 02-9602 RRID: AB_2532969
Secondary peroxidase (HRP)- conjugated anti-rat IgG antibody (for IHC)	Roche Diagnostics	Cat# 760-4457 RRID: AB_3095527
Bacterial and Virus Strains		
Salmonella enterica serovar Typhimurium SL1344	Man et al.[84]	N/A
Influenza A virus A/Puerto Rico/8/34, H1N1 [PR8]	Hoffmann et al.[85]	N/A
Escherichia coli	ATCC	Cat# 11775
Biological Samples		
HEK293T	ATCC	Cat# CRL-3216; RRID: CVCL_0063
Madin-Darby canine kidney cells	ATCC	Cat# CCL-34; RRID:CVCL_0422
Chemicals, Peptides, and Recombinant Proteins		
IMDM	Thermo Fisher Scientific	Cat# 12440053
Fetal bovine serum	Biowest	Cat# S1620
Bovine serum albumin	GoldBio	Cat# A-421-10
Non-essential amino acids	Thermo Fisher Scientific	Cat# 11140-050
Penicillin and streptomycin	Thermo Fisher Scientific	Cat# 15070-063
Lymphoprep™	Stemcell Technologies	Cat# 07801/07811
DMEM	Gibco	Cat# 11995-065
RPMI 1640	Corning	Cat# 10-040-CV
DPBS	Thermo Fisher Scientific	Cat# 14190-250
ATP	Roche	Cat# 101275310001
Poly(dA:dT)	InvivoGen	Cat# tlrl-patn
Xfect reagent	Clonetech Laboratories, Inc	Cat# 631318
Opti-MEM	Thermo Fisher Scientific	Cat# 31985-070
Gentamycin	Thermo Fisher Scientific	Cat# 15750-060
Luria-Bertani media	MP Biomedicals	Cat# 3002-031
Cell conditioning 1 (CC1) buffer	Roche Diagnostics	Cat# 950-500
Hemin	Sigma	Cat# H9039
Pam3CSK4	InvivoGen	Cat# tlrl-pms
Ultrapure LPS from *E. coli* 0111:B4 (in vitro)	InvivoGen	Cat# tlrl-3pelps
R848	InvivoGen	Cat# tlrl-r848
poly(I:C)	InvivoGen	Cat# tlrl-picw
TNF	Preprotech	Cat# 315-01A
Human IFN-γ	Peprotech	Cat# 300-02
Human M-CSF	Peprotech	Cat# 300-25
MCC950	InvivoGen	Cat# inh-mcc

REAGENT or RESOURCE	SOURCE	IDENTIFIER
Z-VAD-FMK	Selleckchem	Cat# S7023
N-acetyl L-cysteine	Sigma	Cat# A9165
Nicotinamide	Sigma	Cat# N3376
Propidium iodide (PI)	Life Technologies	Cat# P3566
Pro-Long™ Diamond Antifade Mountant	Invitrogen	Cat# P36961
Triton X-100	Sigma	Cat# T8787
Normal goat serum	Cell Signaling Technology	Cat# 5425
DAPI (4',6-Diamidino-2-Phenylindole)	Biotium	Cat# 40043
LPS (in vivo)	Sigma	Cat# L2630
Phenylhydrazine	Sigma	Cat# 114715
Poly(I:C) HMW	InvivoGen	Cat# tlrl-pic
Dextran sodium sulfate	Alfa Aesar	Cat# J63606
Protease inhibitor	Roche	Cat# 11697498001
Phosphatase inhibitor	Roche	Cat# 04906837001
Immobilon Forte western HRP substrate	Millipore	Cat# WBLUF0500
SuperSignal™ West Femto Maximum Sensitivity Substrate	Thermo Fisher Scientific	Cat# 34096
EDTA-free protease inhibitor cocktail	Thermo Fisher Scientific	Cat# A32965
Phosphatase inhibitor cocktail	Sigma	Cat# 4906845001
CellROX™ Deep Red Reagent	invitrogen	Cat# C10422
Critical Commercial Assays		
BUN assay	HORIBA	Cat# A11A01641
Creatinine assay	HORIBA	Cat# A11A01933
Iron assay	HORIBA	Cat# A11A01637
ALT assay	HORIBA	Cat# A11A01627
AST assay	HORIBA	Cat# A11A01629
Hemoglobin assay	Oxford science	Cat# VetHemaChemRx
Protein A/G magnetic beads	Thermo Fisher Scientific	Cat# 88802
IL-1β ELISA	Invitrogen	Cat# 88-7013-88
EasySep Direct Human Monocyte isolation kit	Stemcell Technologies	Cat# 19669
Neon™ Transfection System kit	Thermo Fisher Scientific	Cat# MPK5000
Alexa Fluor 594 Antibody Labeling Kit	Thermo Fisher Scientific	Cat# A20185
Deposited Data		
Gene expression in patients with malaria or sickle cell disease	Brito et al.[20]; Idaghdour et al.[21]; Lagresle-Peyrou et al.[22]; Liu et al.[23]	GSE136046, GSE34404 GSE102881, GSE168532
Experimental Models: Organisms/Strains		
Nlrp3$^{-/-}$ mice	Kanneganti et al.[86]	N/A
Nlrp12$^{-/-}$ mice	Zaki et al.[76]	N/A
Nlrc5$^{-/-}$ mice	Kumar et al.[56]	N/A
Nlrc5$^{-/-}$*Nlrp12*$^{-/-}$ mice	This paper	N/A

REAGENT or RESOURCE	SOURCE	IDENTIFIER
Nlrc5-KO^{line2} mice	This paper	N/A
Tlr2$^{-/-}$ mice	Takeuchi et al.[87]	N/A
Tlr4$^{-/-}$ mice	Hoshino et al.[88]	N/A
Tlr2$^{-/-}$ *Tlr4*$^{-/-}$ mice	Sundaram et al.[12]	N/A
Zbp1$^{-/-}$ mice	Ishii et al.[89]	N/A
Nlrc4$^{-/-}$ mice	Mariathasan et al.[90]	N/A
Casp11$^{-/-}$ mice	Kayagaki et al.[91]	N/A
Aim2$^{-/-}$ mice	Jones et al.[92]	N/A
Casp1/11$^{-/-}$ *Ripk3*$^{-/-}$ *Casp8*$^{-/-}$ mice	Gurung et al.[93]	N/A
Casp8$^{-/-}$ *Ripk3*$^{-/-}$ mice	Oberst et al.[94]	N/A
Oligonucleotides		
Non-targeting (control) siRNA	Horizon Discovery	Cat# D-001206-14-20
Mouse-specific *Nlrc5* siRNA	Horizon Discovery	Cat# M-067620-02-0005
Human-specific *NLRC5* siRNA	Horizon Discovery	Cat# M-018267-01-005
pcDNA3-Myc-*hASC*	Addgene	Cat# 73952
pEGFP-C2-*hNLRP3*	Addgene	Cat# 73955
pcDNA3-*hCASP8*	Addgene	Cat# 11817
pcDNA3-HA-*hRIPK3*	Addgene	Cat# 78804
pcDNA3-*hNLRP12*-FLAG	Thermo Fisher Scientific	Cat# V790-20
pcDNA3-*Myc-hNLRC5*	Addgene	Cat# 37509
Software and Algorithms		
GraphPad Prism 9.0 and 10.0	GraphPad Software, Inc.	https://www.graphpad.com/
R package v4.1.1	The Comprehensive R Archive Network	https://cran.r-project.org
Complex Heatmap v2.8.0	Gu et al., 2016	N/A
AUCell v1.18.0 package	Bioconductor	https://bioconductor.org
Halo v3.5	Indica Labs	https://learn.indicalab.com
Leica LAS X software	Leica-microsystems	https://www.leica-microsystems.com/
Fiji	ImageJ	https://imagej.net/ij/